

Effect of regenerator on the direct steam generation solar power system characterized by prolonged thermal storage and stable power conversion

Pengcheng Li^{a, c}, Qing Cao^d, Jing Li^{b,*}, Yandong Wang^e, Gang Pei^f, Cai Gao^a,

Desuan Jie^a, Hongling Zhao^a

^aSchool of Automobile and Traffic Engineering, Hefei University of Technology, 193 Tunxi Road, Hefei, China

^bResearch Center for Sustainable Energy Technologies, Energy and Environment Institute, University of Hull, Hull, HU6 7RX, UK

^cY&C ENGINE CO.,LTD.NO.2 Eqiao Road, Sanshan, Wuhu, China

^dSchool of Mechanical Engineering, Hefei University of Technology, 193 Tunxi Road, Hefei, China

^eHefei General Machinery Research Institute, 888 Changjiang Road ,Hefei, China

^fDepartment of Thermal Science and Energy Engineering, University of Science and Technology of China, 96 Jinzhai Road, Hefei, China

Abstract: The direct steam generation (DSG) solar power system using two stage accumulators and cascade steam-organic Rankine cycle (RC-ORC) has remarkably enlarged storage capacity. It can facilitate stable power generation and address the challenges of conventional DSG systems. Regenerator is generally an issue worthy of discussion of ORC systems. However, its influence on the newly proposed DSG system has not been investigated yet and is expected to be appreciable. Introducing a

regenerator affects not only the ORC efficiency (η_{ORC}), RC-ORC efficiency (η_{RC-ORC}), heat exchanger (HX) area, but also heat storage capacity (W_d), discharge operation duration (t_{ORC}), discharge efficiency ($\eta_{ORC,d}$), aperture area of collectors (A_{col}) and the net profit (ΔP). Detailed performance comparison between the DSG systems without/with regenerator is carried out in this paper. The results indicate that at a given power output, A_{col} is reduced by the regenerator especially for hexamethyldisiloxane (MM), R365mfc and pentane due to the increment in η_{ORC} , η_{RC-ORC} and $\eta_{ORC,d}$ and decrement in the heat input. t_{ORC} is shortened by 0.01-1.78 h depending on ORC fluids. R365mfc exhibits the maximum ΔP (4.19~6.48 million USD), followed by MM (2.82~6.95 million USD). On the contrary, ΔP is negative for benzene (-5.61~-4.31 million USD).

Keywords: regenerator; direct steam generation; heat exchanger area; heat storage capacity; net profit

*Corresponding author. Tel./Fax: +44 (0)1482 463611. E-mail: Jing.Li@Hull.ac.uk

1. Introduction

Direct steam generation (DSG) technology has received increasing attention in concentrating solar power systems. However, its development is restricted by two technical bottlenecks: the instability of steam Rankine cycle (RC) and limited storage capacity. The former is caused by fluctuating solar radiation. The latter is

attributed to the small temperature drop of water in accumulators to avoid inefficient power generation at the off-design condition in the discharge process [1].

In our previous work, an innovative DSG system with two-stage accumulators and cascade steam-organic Rankine cycle (RC-ORC) was proposed, which can solve or alleviate the above challenges [2]. When the system works in nominal condition, water in the low-temperature accumulator (LTA) is heated by solar collectors and partially vaporized to saturated steam to drive the RC-ORC. The unvaporized hot water is stored in the high-temperature accumulator (HTA). By adjusting the mass flow of water from the LTA to the HTA under fluctuating solar radiation, the steam generation rate can keep constant, leading to steady heat-to-power conversion. During discharge water flows from the HTA to the LTA through an intermediate heat exchanger (HX) with a temperature drop of approximately 150~200 °C. The released heat is only used to drive the bottom organic Rankine cycle (ORC). During this period, the HTA undergoes an isothermal process and the storage capacity can be remarkably extended. In principle, the above system differs from existing solar thermal storage technologies. The two-stage accumulators not only combine the advantages of conventional single-stage accumulator and two-tank storage system, but also match the cascade RC-ORC perfectly. Meanwhile, off-design operation of the top RC is avoided and the ORC can work efficiently during the unique heat release process [2].

Regenerator is a common unit and plays a vital role in ORCs. Its influences have been investigated intensively. But most studies only focus on stand-alone ORC systems. Ziviani et al. concluded that the regenerator led to improvements in thermal efficiency,

exergy efficiency, and the outlet temperature of heat source in a subcritical ORC [3, 4]. Meanwhile, regenerative ORC required lower heat to produce the same power than the basic ORC. On the other hand, Ventura et al. revealed that there existed a threshold pressure above which the regenerator did not improve the system performance [5]. As for economics, investigations by Kolahi et al. indicated that the regenerator might increase the payback period, total HX area and capital cost [6, 7]. Braimakis et al. pointed out that recuperative ORC was appealing in some particular conditions [8, 9]. Recent studies and relevant conclusions on regenerator are summarized in Table 1. Besides these theoretical research, ORC manufacturers like Turboden, DürrCyplan, Enertime and Exergy provide the client with commercial-off-the-shelf recuperative systems in biomass and waste heat recovery projects [21-24].

Despite of the importance of regenerator in ORCs, its effect on the newly proposed DSG system has not been assessed. When a regenerator is introduced to the novel system with two-stage accumulators and cascade RC-ORC, current conclusions concerning the effect of regenerator on ORCs may not be applicative. The reasons are as follows: 1) the regenerator influences not only the ORC and RC-ORC efficiencies, power output of RC and ORC, but also heat storage capacity and discharge period; 2) mass flow rates and heat transfer rates in the cascade cycle might be altered and HX area needs to be adjusted accordingly; 3) the changed storage capacity, and cycle efficiencies lead to variations of the heat required by the power block and total aperture area of solar collectors; 4) the annual revenue and net profits in the whole lifetime of the plant are affected consequently.

Thus, it is necessary to conduct an integrated assessment of regenerator's impact on the cascade DSG system. The structure of the work is shown in Fig. 1. '+' and '-' denote increment and decrement, while '+/-' means it could be increment or decrement. Various thermodynamic and thermo-economic indexes without/with regenerator are compared. The economical effect is evaluated by the net profit, which is the sum of extra HX cost, reduced collector cost and generating revenue. The net profits in six regions with representative meteorological conditions are estimated.

2. System description

The schematic diagram of the investigated DSG system is illustrated in Fig. 2. It contains RC, ORC, HTA and LTA. The RC is composed of solar collectors, wet steam turbine and water pumps. The ORC includes a turbine, HX2, regenerator (HX3) and pumps. HX1 serves as a condenser in RC and an evaporator in ORC. The collectors, LTA and HX3 are marked in red, which indicates that HX3 influences the temperature of LTA and the total aperture area of solar collectors. The reasons will be provided in Section 4.

The system can operate in two modes:

- (1) Simultaneous heat collection and power conversion mode (i.e., nominal or rated condition). The system works in this case over a wide range of solar radiation (e.g., 300 -1000 W/m²). Power is generated through the RC-ORC. V1, V2, V4 and V6 are open. P1, P2 and P3 run. The rest valves and pumps are closed or off-work. Water in the LTA is pressurized by P3, heated and partially vaporized through the

collectors. The heated water is stored in the HTA and the saturated steam expands in the wet steam turbine to produce electricity. Afterwards, the exhaust steam is condensed into water by HX1 and is pumped by P1 before being sent back to the collectors. The condensation heat is used to vaporize ORC fluid. The produced saturated vapor expands in the ORC dry turbine to generate electricity. Then, the exhaust vapor is condensed in sequence by HX3 and HX2 into liquid and is ultimately sent back to HX1 by P2. The water flow rate through P3 can be adjusted in dependence on the solar radiation. In this way, constant temperature in HTA and stable power conversion of the RC-ORC are guaranteed.

- (2) Heat discharge mode. V3, V5 are open, and P2 runs. In a conventional DSG system, water in the accumulator is partially vaporized by depressurizing to drive thermodynamic cycle. The temperature drop of water is limited because the wet steam turbines would suffer from inefficient off-design operation [25-26]. However, this flashing process is omitted for the proposed DSG system. The liquid water in HTA flows into LTA via HX1, and the released heat is only used to drive the ORC. This step can generate much more electricity than a conventional discharge process due to the considerable drop in water temperature.

3. Mathematical models

3.1. Thermodynamics

3.1.1. Solar collectors

The solar heat collection is simulated by the System Advisor Model (SAM) software,

which is developed by National Renewable Energy Laboratory [27].

3.1.1.1. Parameter setting in SAM

Collector efficiency (η_{col}) is defined as the optical efficiency (η_{opt}) minus an efficiency penalty term (η_{loss}) representing heat loss [28]:

$$\eta_{col} = \eta_{opt} - \eta_{loss} = K\eta_{opt,0} - \frac{L \cdot q_{loss,av}}{A_{col} \cdot I_{DN}} \quad (1)$$

where K denotes the dependency of η_{opt} on the incidence angle; $\eta_{opt,0}$ is the peak optical efficiency when the incidence angle is zero; L is the length of receivers (m); $q_{loss,av}$ is the average heat loss from evacuated tube receivers (W/m); A_{col} is the aperture area of collectors (m²); I_{DN} is the direct normal solar irradiance (W/m²).

$q_{loss,av}$ is evaluated by

$$q_{loss,av} = a_0 + a_5\sqrt{v_w} + (a_1 + a_6\sqrt{v_w}) \cdot \frac{T_{in} + T_{out} - T_a}{2} + (a_2 + a_4I_{DN}K) \cdot \frac{T_{in}^2 + T_{in}T_{out} + T_{out}^2}{3} + a_3 \frac{(T_{in}^2 + T_{out}^2)(T_{in} + T_{out})}{4} \quad (2)$$

where $a_0 \dots a_6$ are the heat loss coefficients; v_w is the wind speed (m/s); T_{in} and T_{out} are inlet and outlet temperature of the solar field (°C); T_a is the ambient temperature (°C).

The actual operating collectors consist of liquid and binary phase regions. Collector outlet can be at steam-liquid mixture of different dryness with the variation of irradiation intensity, and η_{col} will change accordingly. Collector efficiency in liquid phase region ($\eta_{col,l}$) is determined by

$$\eta_{col,l} = \frac{\dot{m}_{RC} \cdot \Delta h_l}{I_{DN} \cdot A_l} \quad (3)$$

The actual overall collector efficiency is

$$\eta_{col} = \frac{\dot{m}_{RC} \cdot (\Delta h_l + \Delta h_b)}{I_{DN} \cdot (A_l + A_b)} = \frac{\Delta h_l + \Delta h_b}{\frac{\Delta h_l}{\eta_{col,l}} + \frac{\Delta h_b}{\eta_{col,b}}} \quad (4)$$

The specific parameters and the corresponding default values of parabolic trough collectors (PTCs) and linear Fresnel collectors (LFCs) in SAM are posted in Table 2.

For PTCs, K is calculated by

$$K_{PTC} = IAM_{PTC} \cos \theta = \min \left(1, \frac{c_0 \cos \theta + c_1 \theta + c_2 \theta^2}{\cos \theta} \right) \cos \theta \quad (5)$$

where IAM_{PTC} represents the incidence angle modifier; θ is the incidence angle ($^\circ$);

c_0 , c_1 and c_2 are the incidence angle coefficients.

K for LFCs is calculated by

$$K_{LFC} = K_{long} K_{trans} \quad (6)$$

$$K_{long} = c_{0,long} + c_{1,long} \theta_{long} + c_{2,long} \theta_{long}^2 + c_{3,long} \theta_{long}^3 + c_{4,long} \theta_{long}^4 \quad (7)$$

$$K_{trans} = c_{0,trans} + c_{1,trans} \theta_{trans} + c_{2,trans} \theta_{trans}^2 + c_{3,trans} \theta_{trans}^3 + c_{4,trans} \theta_{trans}^4 \quad (8)$$

where θ_{long} and θ_{trans} are the longitudinal and transverse angle ($^\circ$);

$c_{0,long} \dots c_{4,long}$ and $c_{0,trans} \dots c_{4,trans}$ are the incidence angle coefficients. The

default values are indexed in Table 3.

3.1.1.2. Calculation of the incidence angle

When the PTC is north-south oriented with east-west tracking, the incidence angle is calculated by [29]

$$\cos \theta = \sqrt{1 - \cos^2 \alpha_s \cos^2 \gamma_s} \quad (9)$$

where α_s is the solar altitude angle ($^\circ$); γ_s is the solar azimuth angle ($^\circ$).

When the LFC is north-south oriented with east-west tracking, θ_{long} and θ_{trans} are defined as [30]

$$\cos \theta_{long} = \sqrt{1 - \cos^2 \alpha_s \cos^2 \gamma_s} \quad (10)$$

$$\tan \theta_{trans} = \sin \gamma_s / \tan \alpha_s \quad (11)$$

For horizontal PTCs and LFCs, α_s and γ_s are expressed by [31]

$$\sin \alpha_s = \sin \phi \sin \delta + \cos \phi \cos \delta \cos \omega \quad (12)$$

$$\cos \gamma_s = (\sin \alpha_s \sin \phi - \sin \delta) / (\cos \alpha_s \cos \phi) \quad (13)$$

where ϕ is the geographic latitude ($^\circ$), $-90^\circ \leq \phi \leq 90^\circ$; δ is the solar declination ($^\circ$), $-23.45^\circ \leq \delta \leq 23.45^\circ$; ω is the solar hour angle ($^\circ$).

δ is defined by

$$\delta = 23.45 \sin(360 \frac{284+n}{365}) \quad (14)$$

where n represents the n th day in a year, $1 \leq n \leq 365$.

ω is expressed by

$$\omega = 0.25(AST - 720) \quad (15)$$

where AST is the apparent solar time (min) and is determined by

$$AST = LST + ET - 4(SL - LL) \quad (16)$$

where LST is the local standard time (min); ET is the equation of time (min); SL is the standard meridian for the local time zone ($^{\circ}$); LL is the local longitude ($^{\circ}$), $-180^{\circ} \leq LL \leq 180^{\circ}$.

ET is determined by

$$ET = 9.87 \sin 2B - 7.53 \cos B - 1.5 \sin B \quad (17)$$

$$B = 360(n - 81)/365 \quad (18)$$

3.1.2. Turbines

The work produced by the steam and ORC turbines is calculated by

$$\dot{w}_{ST} = \dot{m}_{RC}(h_1 - h_2) = \dot{m}_{RC}(h_1 - h_{2s})\varepsilon_{ST} \quad (19)$$

$$\dot{w}_{OT} = \dot{m}_{ORC}(h_{10} - h_{11}) = \dot{m}_{ORC}(h_{10} - h_{11s})\varepsilon_{OT} \quad (20)$$

where ε_{ST} and ε_{OT} denote the isentropic efficiencies of steam turbine and ORC turbine, respectively.

3.1.3. Heat exchangers

The heat balance in rated condition and discharge process for HX1 is expressed by

$$\dot{m}_{RC}(h_2 - h_3) = \dot{m}_{ORC}(h_{10} - h_{15}) \quad (21)$$

$$\dot{m}_{RC,d}(h_5 - h_6) = \dot{m}_{ORC}(h_{10} - h_{15}) \quad (22)$$

where $\dot{m}_{RC,d}$ is the water mass flow rate through HX1 in discharge process.

The heat balance in HX3 is expressed by

$$h_{11} - h_{12} = h_{15} - h_{14} \quad (23)$$

The regenerator efficiency (ε_r) is defined as [32, 33]

$$\varepsilon_r = \frac{T_{15} - T_{14}}{T_{11} - T_{14}} \quad (24)$$

3.1.4. Pumps

The work consumed by P1 and P2 is calculated by

$$\dot{w}_{P1} = \dot{m}_{RC}(h_4 - h_3) = \dot{m}_{RC}(h_{4s} - h_3)/\varepsilon_P \quad (25)$$

$$\dot{w}_{P2} = \dot{m}_{ORC}(h_{14} - h_{13}) = \dot{m}_{ORC}(h_{14s} - h_{13})/\varepsilon_P \quad (26)$$

where ε_P is the pump isentropic efficiency.

Water flows from HTA to LTA continuously in the heat releasing process to drive the ORC. For further circulation, it is necessary to pump back the water into HTA to supplement the diminishing water. The required pump power is defined as

$$\dot{w}_{P3} = \dot{m}_{RC,d}(h_9 - h_8) = \dot{m}_{RC,d}(h_{9s} - h_8)/\varepsilon_P \quad (27)$$

3.1.5. Heat-to-power conversion efficiency

3.1.5.1. Efficiency under nominal working condition

The RC, ORC and RC-ORC efficiencies are calculated by

$$\eta_{RC} = \frac{\dot{w}_{RC}}{\dot{m}_{RC}(h_1 - h_4)} = \frac{\dot{w}_{ST} \cdot \varepsilon_g - \dot{w}_{P1}}{\dot{m}_{RC}(h_1 - h_4)} \quad (28)$$

$$\eta_{ORC} = \frac{\dot{w}_{ORC}}{\dot{m}_{ORC}(h_{10} - h_{15})} = \frac{\dot{w}_{OT} \cdot \varepsilon_g - \dot{w}_{P2}}{\dot{m}_{ORC}(h_{10} - h_{15})} \quad (29)$$

$$\eta_{RC-ORC} = \frac{\dot{w}_{net}}{Q_{nom}} = \frac{\dot{w}_{RC} + \dot{w}_{ORC}}{\dot{m}_{RC}(h_1 - h_4)} \quad (30)$$

where ε_g is the generator efficiency, \dot{w}_{net} is the net electrical power and Q_{nom} is the heat input in nominal condition.

3.1.5.2. Efficiency during heat discharge

The net generated power by the ORC during heat discharge is expressed by

$$\dot{w}_{ORC,d} = \dot{w}_{OT} \cdot \varepsilon_g - \dot{w}_{P2} - \dot{w}_{P3} \quad (31)$$

The efficiency during heat discharge is calculated by

$$\eta_{ORC,d} = \frac{\dot{m}_{ORC}(h_{10}-h_{11s})\varepsilon_{OT}\cdot\varepsilon_g - \dot{m}_{ORC}\cdot(h_{14s}-h_{13})/\varepsilon_P - \dot{m}_{RC,d}\cdot(h_{9s}-h_8)/\varepsilon_P}{\dot{m}_{ORC}\cdot(h_{10}-h_{15})} \quad (32)$$

The power loss caused by the throttle valve is calculated by

$$\dot{w}_{loss} = \dot{m}_{RC,d} \cdot (h_6 - h_{7s}) \quad (33)$$

The total heat released in this step is defined by

$$Q_d = M_w \cdot (h_5 - h_6) \quad (34)$$

where M_w is the water weight transferred from HTA to LTA, which is the product of water density and HTA volume.

The heat storage capacity (i.e. the power output during discharge) is calculated by

$$W_d = \eta_{ORC,d} \cdot Q_d \quad (35)$$

The operation duration of this process is determined by

$$t_{ORC} = \frac{W_d}{\dot{w}_{ORC,d}} \quad (36)$$

3.2. Thermo-economics

For the convenience of calculation, the rated net power is assumed to be constant without and with the regenerator ($\dot{w}_{net} = \dot{w}_{net,r} = 10 \text{ MW}$). The comparison is made at the same volume of accumulators. According to the conservation of energy, the total heat output from the solar field is equal to the total heat input to the power block in both rated operation and discharge process during a typical meteorological year. The duration of the nominal condition (t_{RC-ORC}) is not affected by the regenerator since the rated power and meteorology conditions are the same for a given region. Therefore, the power output under nominal condition in the typical meteorological year is fixed. Besides, the initial investment in turbines is considered to be independent of the regenerator due to the constant power capacity.

The regenerator mainly influences the discharge duration (t_{ORC}), power output in discharge process, HX area and its cost. It also affects the solar aperture area and its cost because the daily heat input to the power block varies and thus the design aperture area needs adjustment. The daily heat requirement for the RC-ORC is determined by two parameters: the heat-to-power conversion efficiency in the nominal operation and the heat release in the discharge process. Both parameters are elevated by the regenerator.

3.2.1. HX area

HTRI software, which is considered to be the industry's most advanced thermal process design and simulation software [34], is used to estimate the HX area. Calculation procedure of the required HX area in HTRI is given by Eqs. (37)~(43).

HX area is expressed as

$$A = \frac{Q}{U\Delta T_m} \quad (37)$$

where Q is the heat duty in HX.

The mean temperature difference (ΔT_m) can be written as

$$\Delta T_m = \frac{\Delta T_{in} - \Delta T_{out}}{\ln\left(\frac{\Delta T_{in}}{\Delta T_{out}}\right)} \quad (38)$$

The effect of heat conductivity is ignored and the overall heat transfer coefficient U is calculated as

$$\frac{1}{U} = \frac{1}{U_{shell}} + \frac{1}{U_{tube}} \quad (39)$$

Heat transfer coefficient in single-phase is given by the Petuk-hov correlation [35]

$$U_s = \frac{k}{D} \left(\frac{\frac{f}{8} \cdot Re \cdot Pr}{12.7 \left(\frac{f}{8}\right)^{0.5} \left(Pr^{\frac{2}{3}} - 1\right) + 1.07} \right) \quad (40)$$

where f is Darcy resistance coefficient, and it is calculated by Filonenko equation

$$f = \frac{1}{(1.82 \lg Re - 1.64)^2} \quad (41)$$

For boiling heat transfer, the coefficient in binary-phase region developed by Gungor and Winterton is used [36]

$$U_b = 0.023 \left[\frac{G(1-\chi)d}{\mu} \right]^{0.8} Pr^{0.4} \frac{k}{d} \left[1 + 3000Bo^{0.86} + 1.12 \left(\frac{\chi}{1-\chi} \right)^{0.75} \left(\frac{\rho_l}{\rho_v} \right)^{0.41} \right] \quad (42)$$

For condensation heat transfer, the coefficient in binary-phase region is given by Shah [37]

$$U_c = 0.023 \left[\frac{G(1-\chi)d}{\mu} \right]^{0.8} Pr^{0.4} \frac{k}{d} \left[(1-\chi)^{0.8} + \frac{3.8\chi^{0.76}(1-\chi)^{0.04}}{Pr^{0.38}} \right] \quad (43)$$

3.2.2. Cost of extra HX area (ΔC_{HX})

Purchased cost of HX is [38, 39, 40]

$$\log_{10} C_p = K_1 + K_2 \log_{10} A + K_3 (\log_{10} A)^2 \quad (44)$$

where C_p is a basic cost concerning with the HX area. Considering the specific material of the construction and operating pressure, the bare module cost for HX should be corrected as [38, 39, 40]

$$C_{BM} = C_p (B_1 + B_2 F_M F_p) \quad (45)$$

C_{BM} is the corrected cost, F_M is the material correction factor, and F_p is a measure that reflects the pressure factor since the system components work at a pressure much higher than the ambient pressure, which is determined by [38, 39, 40]

$$\log_{10} F_p = C_1 + C_2 \log_{10} (10p - 1) + C_3 [\log_{10} (10p - 1)]^2 \quad (46)$$

K_1 , K_2 , K_3 , B_1 , B_2 , C_1 , C_2 and C_3 are coefficients for the cost evaluation of system components. The values are posted in Table 4. Since the unit in the parentheses of the second term in the right hand side of Eq. (46) is gage pressure in bar, a transformation from MPa to bar is thus needed to fit the equation request.

The actual cost need to be converted from the cost of 2001 by introducing the Chemical Engineering Plant Cost Index (*CEPCI*) [41]. The cost of 2014 should be corrected as

$$C_{BM,2014} = C_{BM,2001} \square CEPCI_{2014} / CEPCI_{2001} \quad (47)$$

where $CEPCI_{2001}=397$, $CEPCI_{2014}=586.77$.

The cost of extra HX area is

$$\Delta C_{HX} = (C_{BM,HX1,2014} + C_{BM,HX2,2014} + C_{BM,HX3,2014})_r - (C_{BM,HX1,2014} + C_{BM,HX2,2014}) \quad (48)$$

3.2.3. Variation of collector cost (ΔC_{col})

The varied aperture area (ΔA_{col}) is composed of the reduced area in nominal condition ($\Delta A_{col,nom}$) and the reduced area in heat discharge ($\Delta A_{col,d}$). ΔA_{col} can be obtained according to the conservation of energy:

$$\Delta A_{col} = \Delta A_{col,nom} + \Delta A_{col,d} = \frac{\sum_{j=0}^{365} \Delta(Q_{nom,j} + Q_{d,j})}{\sum_{i=0}^{8760} \eta_{col,i} \square I_{DN,i}} \quad (49)$$

where $\Delta(Q_{nom,j} + Q_{d,j})$ is the variation of daily required heat. $\eta_{col,i}$ and $I_{DN,i}$ is hourly collector efficiency and direct normal radiation, respectively. $\eta_{col,i}$ varies little for the system without or with a regenerator, and the reason will be provided in Section 4.1.2.

The reduced cost of solar collectors is expressed by

$$\Delta C_{col} = P_{col} \cdot \Delta A_{col} \quad (50)$$

where P_{col} is the collector price per square meter, including costs of manufacturing, assembly, equipment and construction activities. The annual operation and maintenance cost is not considered and ΔC_{col} is conservative estimated.

3.2.4. Net profit with respect to the regenerator (ΔP)

The additional yield in the whole lifetime (LT) of the plant is determined by

$$\Delta Y = P_e \cdot \Delta W_d \cdot 365 \cdot LT \quad (51)$$

where P_e is the electricity price, ΔW_d is the variation of storage capacity during heat discharge due to the installation of regenerator.

The net profit by the regenerator (ΔP) is expressed by

$$\Delta P = \Delta Y + \Delta C_{col} - \Delta C_{HX} \quad (52)$$

4. Results and discussion

The effects of ORC fluids on the system performance are studied. Pentane is a popular working fluid adopted by Ormat Technologies Inc. [45], which has built more than 1000 ORC plants of up to 1701 MW [46]. Therefore, it is selected as the representative fluid. Then benzene, cyclohexane, R1233zd-E, hexamethyldisiloxane (MM) and R365mfc are analyzed. R1233zd-E is a new promising fluid with low global warming potential and almost no ozone depletion potential. Experimental investigation shows that it is a drop-in replacement for R245fa [47-49]. The physical property parameters of R1233zd-E can be obtained from AP1700 [50]. MM has favorable thermal stability and is suitable for high temperature ORC [51-52]. Research indicates MM is one of the best ranked fluids because of its high efficiency and environmental friendliness [53]. Benzene, cyclohexane and R365mfc are widely investigated with high efficiencies and good feasibilities [54-55].

Only subcritical cycles are considered, which offer a constant temperature and pressure in the vaporization process. The assumptions in the calculation are shown in Table 5. In the event of a market price from China, a current exchange rate from China Renminbi to US dollar (USD) of 0.16 is applied.

4.1. Thermodynamic performance using pentane

4.1.1. Thermodynamic performance under nominal condition

Wet steam turbines in a commercial nuclear plant, Qinshan Nuclear Power Plant (300 MW, China), is served as reference [58]. In this simulation, the wet steam turbine in the RC has the same design outlet pressure as the high pressure turbine in Qinshan Nuclear Power Plant (0.817 MPa). The results of the calculated parameters in the bottom cycle are listed in Table 6.

Design conditions of thermodynamic performance without/with regenerator are displayed in Table 7. The RC efficiency (η_{RC}) remains invariable owing to the fixed design parameters of RC. By installing the regenerator, the ORC efficiency (η_{ORC}) increases by 16.4% while the RC-ORC efficiency (η_{RC-ORC}) improves by 9.7%. Besides, the output of RC (\dot{w}_{RC}) declines by 0.36 MW, and the output of ORC (\dot{w}_{ORC}) increases by 0.36 MW as compensation. The fluctuations of both the mass flow rates of RC (\dot{m}_{RC}) and ORC (\dot{m}_{ORC}) are within 10%. Notably, heat input (Q_{nom}) is 3.71 MW less than that of no regenerator. It indicates that less heat is required by using regenerator at a rated power. Therefore, thermodynamic performance of the system can be improved appreciably by the regenerator.

4.1.2. Thermodynamic performance in the heat discharge process

T - Q diagram during heat discharge is depicted in Fig. 3, which reveals the relationship between fluid temperature and heat transfer rate in HX1. The specific enthalpy of Point 5' (the state point of water corresponds to the ORC fluid's saturated liquid state) can be obtained by solving the heat balance equation on latent or sensible heat sections of HX1. The place where the minimum temperature difference ($\Delta T_{min}=10$ °C) occurs is at the cold fluid inlet, which is the same as that without regenerator [2].

The bottom ORC operates under rated condition in the heat discharge process. The related parameters are listed in Table 8. The discharge duration (t_{ORC}) is shortened by 0.87 h due to the regenerator. More work is consumed by P3 and throttling process on account of the increased discharge mass flow rate of water ($\dot{m}_{RC,d}$) from the HTA to LTA. The raise in discharge ORC efficiency ($\eta_{ORC,d}$) is 16.3%. Notably, the storage capacity (W_d) drops by 714.6 kWh, which can be explained by an insight to the parameter distribution of the top water. As shown in Table 9, T_6 elevates after employing the regenerator. The reduction of enthalpy drop of water ($h_5 - h_6$) is significant, leading to a decreased heat in discharge (ΔQ_d).

Variation of PTC efficiency (η_{PTC}) with the solar field outlet dryness is graphed in Fig. 4. Given I_{DN} , η_{PTC} decreases slightly with the increment of outlet dryness. As the outlet dryness increases from 0 to 1, the relative decrement is only 0.74%, 0.98% and 1.46% when I_{DN} is 800, 600 and 400 W/m², respectively. The reason is that PTC

efficiency in binary phase region ($\eta_{PTC,b}$) declines marginally as compared with that in liquid phase region ($\eta_{PTC,l}$). Similarly, the outlet dryness also has minimal effect on η_{LFC} . Besides, given I_{DN} ($800\text{W}/\text{m}^2$), the two curves representing different inlet temperatures almost coincide. It manifests the regenerator has little impact on η_{col} . Therefore the fluctuation of T_{in} has little effect on the yearly heat collection ($\sum_{i=0}^{8760} \eta_{col,i} I_{DN,i}$). For instance, in the regenerative case the heat for Phoenix is 1642.02 and 1084.82 $\text{kWh}/\text{m}^2 \cdot \text{year}$ by PTC and LFC, respectively. It is 1644.48 and 1086.00 $\text{kWh}/\text{m}^2 \cdot \text{year}$ in non-recuperated case. The difference is slight. $\eta_{col,i}$ in Eq. (49) can be the hourly collector efficiency independent on the regenerator.

4.2. Thermo-economic performance using pentane

4.2.1. Cost of extra HX area

Employing regenerator will inevitably elevate the total HX cost. Large HX cost is mainly contributed by its area and hence total amount of materials in use [59, 60]. All the adopted HXs are single shell and double tube pass heat exchangers. The tube outer diameter of 19 mm and tube pitch of 25 mm are adopted, which are common in industrial production. Shell and tube HX shows great flexibility in terms of heat power transferred between hot and cold fluids, high operating pressure and temperature, great availability of construction materials, high value of both heat power transferred/weight and volume ratio and finally low costs [61, 62]. Hot fluid is located in shell side and cold fluid is in tube side. Over design area of approximately 5~10% is ensured. Flow chart of the HX area calculation is exhibited in Fig. 5.

Key parameters of the HXs in rated conditions are indexed in Table 10. As the inlet pressure of HX2 at shell side (P_{12}) is low, the enhancement in heat transfer by increasing the flow rate is limited by pressure drop, and thus rod baffle is adopted in HX2 to reduce the vibration and the flow resistance of the shell side fluid. The design inlet mass flow rate and temperature of HX1 at the tube side increases after introducing HX3. Accordingly, some design parameters of HX1 are altered slightly but its area can meet the heat transfer requirement in regenerative situation. In addition, the heat duty of HX2 decreases because part of the condensing heat duty is shared by HX3. As a result, HX2 area is reduced. The total cost of HXs is increased by 0.563 million USD after employing the regenerator.

4.2.2. Reduced cost of collectors and the net profit

Direct normal irradiance in a typical meteorological day (vernal equinox day) derived from EnergyPlus [63] is graphed in Fig. 6. Phoenix is exemplified and the collector efficiency is also exhibited. η_{PTC} is considerably higher than η_{LFC} . In practical operation, simultaneous heat collection and power conversion mode switches on when $I_{DN} \geq 400 \text{ W/m}^2$ in the morning and it ceases when the last hourly $I_{DN} \geq 400 \text{ W/m}^2$ appears. The system works in this mode from 9:00 to 18:00 and t_{RC-ORC} is 9 h. According to the data in EnergyPlus, the yearly t_{RC-ORC} of 3056, 2515, 2333, 2020, 2792 and 1726 h can be determined for Phoenix, Sacramento, Cape Town, Canberra, Lhasa and Delingha, respectively.

The reduced aperture area (ΔA_{col}) and net profits are depicted in Fig. 7. ΔA_{LFC} is

appreciably larger than ΔA_{PTC} on account of the lower η_{LFC} and less $\sum_{i=0}^{8760} \eta_{col,i} \square I_{DN,i}$.

ΔA_{col} in Delingha is the largest owing to the least $\sum_{i=0}^{8760} \eta_{col,i} \square I_{DN,i}$. Given the region, ΔP_{LFC} is slightly higher than ΔP_{PTC} , which indicates that regenerator is more beneficial in the LFC-based system. ΔP is the greatest in Delingha, where the direct radiation resource is least among the six regions. On the contrary, the lowest ΔP is contributed by the most abundant solar irradiance region of Phoenix. It is more profitable to install regenerator in the territories with weaker solar radiation resources.

4.3. Thermodynamic performance using other five ORC fluids

4.3.1. Thermodynamic performance under nominal condition

Parameters under nominal conditions for the five ORC fluids (benzene, cyclohexane, R1233zd-E, MM and R365mfc) are provided in Table 11. Compared with those of non-recuperated situations, η_{ORC} increases by 4.62%, 12.83%, 0.40%, 39.59% and 18.36% for benzene, cyclohexane, R1233zd-E, MM and R365mfc, respectively. The corresponding variations of η_{RC-ORC} are -0.22%, 7.91%, 0.20%, 20.66% and 10.66%. Regenerator has no effect on \dot{w}_{RC} and \dot{w}_{ORC} for benzene but results in lower η_{RC-ORC} and higher Q_{nom} . The wet steam turbine is less efficient than the ORC turbine and a higher mass flow rate of water/steam in the RC might not be beneficial. \dot{w}_{ORC} climbs by 0.28, 0.01, 0.82 and 0.40 MW in sequence for the rest four fluids and the corresponding Q_{nom} declines by 2.88, 0.09, 7.25 and 4.12 MW. In particular, \dot{m}_{RC} decreases and \dot{m}_{ORC} elevates except for benzene. The data show that

thermodynamic performance is promoted significantly by using MM, while the improvements are appreciable for cyclohexane and R365mfc. The influence is minor for R1233zd-E and even negative for benzene.

4.3.2. Thermodynamic performance in heat discharge process

T - Q diagrams during heat discharge are depicted in Fig. 8. As a hot side fluid, water leaves HTA at a constant temperature (250 °C), but reaches LTA inlet at different temperatures. The heat transfer is related to the characteristics of ORC fluids. ΔT_{min} appears at the saturated liquid state for benzene and cyclohexane, while it takes place at the cold fluid inlet for R1233zd-E, MM and R365mfc. The reason is that the latent heat values of benzene and cyclohexane are larger, and most of the absorbed heat is used for evaporation. It results in a relatively high average temperature of the hot side fluid. For instance, the ratio of specific latent heat in the vaporization process to the total absorbed heat (i.e., $h_{10} - h_{15}$) is 59.3% for benzene, while it is only 42.5% for pentane.

The increased storage capacity is provided in Table 12. t_{ORC} is shortened by 0.76, 0.48, 0.01, 1.78 and 0.77 h in sequence to complete the discharge process by the employment of regenerator. The consumed work by P3 (\dot{w}_{p3}) and the power loss in the throttling process (\dot{w}_{loss}) are greater in the regenerative case (except for \dot{w}_{p3} using cyclohexane) mainly due to the increased $\dot{m}_{RC,d}$. $\eta_{ORC,d}$ increases by 4.50%, 13.09%, 0.41%, 39.05% and 18.62% after adopting the regenerator. W_d climbs by 156.1 kWh for cyclohexane, 4.6 kWh for R1233zd-E and 554.6 kWh for R365mfc, while it declines

by 4737.8 kWh for benzene and 969.7 kWh for MM. The decreased W_d can be explained by the parameters in Table 13. The temperature of water (T_6) in the LTA is elevated by the regenerator. ΔT_6 is 18.05 °C for benzene and is even larger when the fluid is MM. The total heat released from the HTA to LTA is thereby reduced. Due to the trade-off between $\Delta \eta_{ORC,d}$ and ΔT_6 , W_d might drop. The above results demonstrate that the regenerator improves thermodynamic indexes significantly in discharge process for cyclohexane and R365mfc, but affects R1233zd-E marginally. Though the regenerator elevates $\eta_{ORC,d}$ for benzene and MM, its negative effects on W_d is evident.

4.4. Thermo-economic performance using the five ORC fluids

Parameters of the HXs without/with regenerator are displayed in Tables 15 and 16. Compared with the corresponding data in Table 15, HX1 area in Table 16 keeps constant while HX2 area decreases. Notably, as the hot fluid inlet of HX3 (P_{11}) for MM is low (only 9 kPa), rod baffle will be required to reduce flow resistance if the hot fluid is located in shell side, leading to dramatically huge shell size and expensive HX. To avoid such situation cold fluid is located in shell side because the velocity of liquid is much lower than that of vapor, which leads to large allowable pressure drop. Single baffle is employed to guarantee high heat transfer coefficient and acceptable HX area. Conversely, HX3 area for R1233zd-E is small due to the low heat duty and high overall heat transfer coefficient. The total area in Table 16 expands by 27.02%, 43.35%, -5.86%, 158.14% and 27.32% successively. The corresponding extra initial investment on heat exchangers is 0.812, 1.073, 0.020, 3.240 and 0.674 million USD.

ΔA_{col} and the net profits for benzene are depicted in Fig. 9. It's worth noting that ΔP_{PTC} and ΔP_{LFC} are negative in all the regions (-5.61~-4.31 million USD), which manifests that the regenerator has adverse economic effect. Similar with Fig. 6, both ΔA_{PTC} and ΔA_{LFC} in Delingha is the most striking, and the least is in Phoenix. In addition, given the territory, the difference between ΔP_{PTC} and ΔP_{LFC} is not significant in both Figs. 6 and 9. Therefore, only PTC is exemplified in Figs. 10 and 11, which show ΔA_{PTC} and the net profits for the rest four fluids. It is observed that ΔA_{PTC} for MM is the most ($4.33\sim 6.76 \times 10^4 \text{ m}^2$), followed by R365mfc and cyclohexane. R365mfc exhibits the maximum net profits (4.19~6.48 million USD), followed by MM (2.82~6.95 million USD). The least ΔA_{PTC} of approximately $0.05\sim 0.08 \times 10^4 \text{ m}^2$ and the lowest net profits of 0.07~0.13 million USD are achieved for R1233zd-E, which indicates that the regenerator has little benefits for R1233zd-E. ΔP is the maximum in relatively low irradiation district of Delingha while the minimum appears in Phoenix. It follows that the regenerator produces less profits in areas with richer solar radiation resources.

5. Conclusion

The effect of regenerator on the DSG cascade solar power system characterized by two-stage accumulators and unique prolonged thermal storage is investigated. The performances in the rated condition and the discharge process are analyzed. Comprehensive impacts of various thermodynamic and thermo-economic indicators are compared. Following conclusions can be drawn:

(1) In the nominal condition, η_{ORC} and η_{RC-ORC} may be raised by using regenerator. The efficiency increment is most appreciable for MM, followed by pentane, cyclohexane and R365mfc. However, the regenerator effect on efficiency is minor for R1233zd-E and can be negative for benzene (η_{RC-ORC} declines by 0.22% and 0.08 MW more heat is required by the power block).

(2) In the discharge process, the extent of the enhancement in $\eta_{ORC,d}$ is similar with that of η_{ORC} in the rated condition. t_{ORC} is shortened by 0.87, 0.76, 0.48, 0.01, 1.78 and 0.77 h in sequence for pentane, benzene, cyclohexane, R1233zd-E, MM and R365mfc due to the regenerator. W_d declines by 4737.8 kWh for benzene, 714.6 kWh for pentane and 969.7 kWh for MM, while it goes up by 156.1 kWh for cyclohexane, 4.6 kWh for R1233zd-E and 554.6 kWh for R365mfc.

(3) The required HX1 area keeps constant while the HX2 area decreases when the regenerator is introduced. The maximum extra initial investment in HXs is 3.24 million USD for MM, and the minimum is 0.02 million USD for R1233zd-E. The most ΔA_{PTC} of approximately $4.33 \sim 6.76 \times 10^4 \text{ m}^2$ can be saved for MM, while the least of approximately $0.05 \sim 0.08 \times 10^4 \text{ m}^2$ is achieved for R1233zd-E. ΔP_{LFC} is slightly higher than ΔP_{PTC} , which indicates that the regenerator is more advantageous in the LFC-based system.

(4) R365mfc exhibits the maximum ΔP (4.19~6.48 million USD), followed by MM (2.82 ~ 6.95 million USD). Notably, ΔP is inappreciable for R1233zd-E (0.07~0.13 million USD) and negative for benzene (-5.61~-4.31 million USD). It

manifests that the regenerator has trivial effect for R11233zd-E and negative impact for benzene. Finally, it is less profitable to employ regenerator in territories with more abundant direct radiation resources such as Phoenix.

Acknowledgment

This study was sponsored by EU Marie Curie International Incoming Fellowships Program (703746), Fundamental Research Funds from Hefei University of Technology (Grant No. 407-0371000083), National Natural Science Foundation of China (Grant No. 51876053)

References

- [1] Gao GT, Li J, Li PC, Cao JY, Pei G, Dabwan YN, Su YH. Design of steam condensation temperature for an innovative solar thermal power generation system using cascade Rankine cycle and two-stage accumulators. *Energy Conv Manag* 2019; 184: 389-401.
- [2] Li J, Gao GT, Kutlu C, Liu KL, Pei G, Su YH, Ji J, Riffat S. A novel approach to thermal storage of direct steam generation solar power systems through two-step heat discharge. *Appl Energy* 2019; 236: 81-100.

- [3] Ziviani D, Groll EA, Braun JE, Paepe MD, Broek M. Analysis of an organic Rankine cycle with liquid-flooded expansion and internal regeneration (ORCLFE). *Energy* 2018; 144: 1092-106.
- [4] Anvari S, Jafarmadar S, Khalilarya S. Proposal of a combined heat and power plant hybridized with regeneration organic Rankine cycle: Energy-Exergy evaluation. *Energy Conv Manag* 2016; 122: 357-65.
- [5] Ventura C, Rowlands AS. Recuperated power cycle analysis model: Investigation and optimisation of low-to-moderate resource temperature Organic Rankine Cycles. *Energy* 2015; 93: 484-94.
- [6] Kolahi M, Yari M, Mahmoudi S, Mohammadkhani F. Thermodynamic and economic performance improvement of ORCs through using zeotropic mixtures: Case of waste heat recovery in an offshore platform. *Case Study Therm Eng* 2016; 8: 51-70.
- [7] Feng YQ, Zhang YN, Li BX, Yang JF, Shi Y. Comparison between regenerative organic Rankine cycle (RORC) and basic organic Rankine cycle (BORC) based on thermoeconomic multi-objective optimization considering exergy efficiency and levelized energy cost (LEC). *Energy Conv Manag* 2015; 96: 58-71.
- [8] Braimakis K, Karellas S. Integrated thermoeconomic optimization of standard and regenerative ORC for different heat source types and capacities. *Energy* 2017; 121: 570-98.
- [9] Li G. Organic Rankine cycle performance evaluation and thermoeconomic assessment with various applications part II: economic assessment aspect. *Renewable*

Sustainable Energy Rev 2016; 64: 490-505.

[10] Ge Z, Wang H, Wang HT, Wang JJ, Li M, Wu FZ, Zhang SY. Main parameters optimization of regenerative organic Rankine cycle driven by low-temperature flue gas waste heat. Energy 2015; 93: 1886-95.

[11] Zhu YD, Hu Z, Zhou YD, Jiang L, Yu LJ. Discussion of the internal heat exchanger's effect on the Organic Rankine Cycle. Appl Therm Eng 2015; 75: 334-43.

[12] Hajabdollahi H, Ganjehkaviri A, Jaafar MNM. Thermo-economic optimization of RSORC (regenerative solar organic Rankine cycle) considering hourly analysis. Energy 2015; 87: 369-80.

[13] Zhang C, Liu C, Xu XX, Li QB, Wang SK, Chen X. Effects of superheat and internal heat exchanger on thermo-economic performance of organic Rankine cycle based on fluid type and heat sources. Energy 2018; 159: 482-95.

[14] Liu P, Shu GQ, Tian H. How to approach optimal practical Organic Rankine cycle (OP-ORC) by configuration modification for diesel engine waste heat recovery. Energy 2019; 174: 543-52.

[15] Reza K, Hadi G, Mohammad E, Hadi R. Thermodynamic modeling and performance analysis of four new integrated organic Rankine cycles (A comparative study). Appl Therm Eng 2017; 122: 103-17.

[16] Bina SM, Jalilinasrabady S, Fujii H. Energy, economic and environmental (3E) aspects of internal heat exchanger for ORC geothermal power plants. Energy 2017; 140:

1096-106.

[17] Braimakis K, Karellas S. Energetic optimization of regenerative Organic Rankine Cycle (ORC) configurations. *Energy Conv Manag* 2018; 159: 353-70.

[18] Javanshir A, Sarunac N, Razzaghpanah Z. Thermodynamic analysis of a regenerative organic Rankine cycle using dry fluids. *Appl Therm Eng* 2017; 123: 852-64.

[19] Tiwari D, Sherwani AF, Atheaya D, Arora A. Energy and exergy analysis of solar driven recuperated organic Rankine cycle using glazed reverse absorber conventional compound parabolic concentrator (GRACCPC) system. *Sol Energy* 2017; 155: 1431-42.

[20] Habibi H, Chitsaz A, Javaherdeh K, Zoghi M, Ayazpour M. Thermo-economic analysis and optimization of a solar-driven ammonia-water regenerative Rankine cycle and LNG cold energy. *Energy* 2018; 149: 147-60.

[21] Turboden biomass. Working Principle,
https://www.turboden.com/upload/blocchi/X12837allegato1-7929X_Turboden_Biomass.pdf; [accessed 6 August 2019].

[22] Dürr Electricity generation from waste heat. Product overview,
https://www.durr-cyplan.com/fileadmin/durr-cyplan.com/07_Broschueren/duerr-orc-brochure-en.pdf; [accessed 6 August 2019].

[23] Enertime. ORC modules, <https://www.enertime.com/en/technology/solutions/orc->

modules; [accessed 6 August 2019].

[24] EXERGY. Application, <http://exergy-orc.com/application/heat-recovery-from-industrial-process>; [accessed 6 August 2019].

[25] Steinmann WD, Eck M. Buffer storage for direct steam generation. *Sol Energy* 2006; 80: 1277-82.

[26] Casati E, Galli A, Colonna P. Thermal energy storage for solar-powered organic Rankine cycle engines. *Sol Energy* 2013;96:205-19.

[27] NREL.System Advisor Model, <http://sam.nrel.gov/>; [accessed 6 August 2019].

[28] NREL. System Advisor Model User Documentation, Help Contents. Version 2017.9.5.

[29] Kalogirou S. Parabolic trough collector system for low temperature steam generation: Design and performance characteristics. *Appl Energy* 1996; 55: 1-19.

[30] Morin G, Dersch J, Platzer W, Eck M, Häberle A. Comparison of Linear Fresnel and Parabolic Trough Collector power plants. *Sol Energy* 2012; 86: 1-12.

[31] Duffie JA, Beckman WA. *Solar Engineering of Thermal Processes*. 4th ed. John Wiley & Sons; 2013.

[32] Tchanche BF, Lambrinos G, Frangoudakis A, Papadakis G. Exergy analysis of micro-organic Rankine power cycles for a small scale solar driven reverse osmosis desalination system. *Appl Energy* 2010; 87: 1295-306.

[33] Pei G, Li J, Ji J. Analysis of low temperature solar thermal electric generation using

regenerative Organic Rankine Cycle. *Appl Therm Eng* 2010; 30: 998-1004.

[34] HTRI Software, <http://www.htri.net>; [accessed 24 November 2019].

[35] F.P. Incropera, D.P. Dewit, *Fundamentals of Heat and Mass Transfer*, fifth ed., John Wiley and Sons, New York, 2002.

[36] A.E. Gungor, R.H.S. Winterton, Simplified general correlation for saturated flow boiling and comparisons for correlations with data, *Chemical Engineering Research and Design* 65 (1987) 148-156.

[37] M.M. Shah, A general correlation for heat transfer during film condensation inside pipes, *International Journal of Heat and Mass Transfer* 22 (1979) 547-556.

[38] Li YR, Du MT, Wu CM, Wu SY, Liu C, Xu JL. Economical evaluation and optimization of subcritical organic Rankine cycle based on temperature matching analysis. *Energy* 2014; 68: 238-47.

[39] Turton R, Bailie RC, Whiting WB, Shaeiwit JA. *Analysis, synthesis, and design of chemical processes*. 4th ed. Prentice Hall PTR; 2013.

[40] Zhang C, Liu C, Wang SK, Xu XX, Li QB. Thermo-economic comparison of subcritical organic Rankine cycle based on different heat exchanger configurations. *Energy* 2017; 123: 728-41.

[41] Turton R, Bailie RC, Whiting WB, Shaeiwit JA. *Analysis, synthesis, and design of chemical processes*. Pearson Education Inc; 2009.

[42] Kurup P, Turchi CS. Parabolic Trough Collector Cost Update for the System

Advisor Model (SAM). NREL/TP-6A20-65228; 2015.

[43] LFCs by Beijing TeraSolar Photothermal Technologies Co., Ltd., <http://www.terasolar.com.cn/>; [accessed 6 August 2019].

[44] Benchmark Feed-in-Tariff policy of solar thermal power industry in China, <https://en.cspplaza.com/>; [accessed 01 November 2017].

[45] Li J. Gradual progress in the organic rankine cycle and solar thermal power generation. In: Li J, editor. Structural optimization and experimental investigation of the organic rankine cycle for solar thermal power generation. Springer Theses. Springer; 2015.

[46] Tartière T, Astolfi M. A world overview of the organic Rankine cycle market. *Energy Proc* 2017; 129: 2-9.

[47] Eyerer S, Wieland C, Vandersickel A, Spliethoff H. Experimental study of an ORC (Organic Rankine Cycle) and analysis of R1233zd-E as a drop-in replacement for R245fa for low temperature heat utilization. *Energy* 2016; 103: 660-671.

[48] Eyerer S, Dawo F, Kaindl J, Wieland C, Spliethoff H. Experimental investigation of modern ORC working fluids R1224yd(Z) and R1233zd(E) as replacements for R245fa. *Appl Energy* 2019; 240: 946-963.

[49] Yang JY, Ye ZH, Yu BB, Ouyang HS, Chen JP. Simultaneous experimental comparison of low-GWP refrigerants as drop-in replacements to R245fa for Organic Rankine cycle application: R1234ze(Z), R1233zd(E), and R1336mzz(E). *Energy* 2019;

173: 721-731.

[50] <http://www.ap1700.com/default.aspx> [accessed 24 November 2019].

[51] Preißinger M, Brüggemann D. Thermal stability of hexamethyldisiloxane (MM) for high-temperature Organic Rankine Cycle (ORC). *Energies* 2016; 9: 183.

[52] Preißinger M, Brüggemann D. Thermo-economic evaluation of modular organic rankine cycles for waste heat recovery over a broad range of heat source temperatures and capacities. *Energies* 2017; 10: 269.

[53] Preißinger M, Schwöbel JAH, Klamt A, Brüggemann D. Multi-criteria evaluation of several million working fluids for waste heat recovery by means of organic Rankine cycle in passenger cars and heavy-duty trucks. *Appl Energy* 2017; 206: 887-899.

[54] Fergani Z, Touil D, Morosuk T. Multi-criteria exergy based optimization of an Organic Rankine Cycle for waste heat recovery in the cement industry. *Energy Conv Manag* 2016; 112: 81-90.

[55] Song J, Gu CW. Parametric analysis of a dual loop Organic Rankine Cycle (ORC) system for engine waste heat recovery. *Energy Conv Manag* 2015; 105: 995-1005.

[56] Shu GQ, Liu P, Tian H, Wang X, Jing DZ. Operational profile based thermal-economic analysis on an Organic Rankine cycle using for harvesting marine engine's exhaust waste heat. *Energy Conv Manag* 2017; 146: 107-123.

[57] Li P, Han ZH, Jia XQ, Mei ZK, Han X, Wang Z. Comparative analysis of an organic Rankine cycle with different turbine efficiency models based on multi-objective

optimization. *Energy Conv Manag* 2019; 185: 130-142.

[58] Zou JM. Analysis on Erosion and Corrosion in QNPC 300MW Turbine. *Turbine Technol* 2003; 45: 180-2.

[59] Hettiarachchi HDM, Golubovic M, Worek WM, Ikegami Y. Optimum design criteria for an Organic Rankine cycle using low-temperature geothermal heat sources. *Energy* 2007; 32: 1698-706.

[60] Cataldo F, Mastrullo R, Mauro AW, Vanoli GP. Fluid selection of organic Rankine cycle for low-temperature waste heat recovery based on thermal optimization. *Energy* 2014; 72: 159-67.

[61] Shah RK, Sekulic DP. *Fundamentals of Heat Exchanger Design*. Wiley; 2003.

[62] Calise F, Capuozzo C, Carotenuto A, Vanoli L. Thermo-economic analysis and off-design performance of an organic Rankine cycle powered by medium-temperature heat sources, *Sol Energy* 2014; 103: 595-609.

[63] EnergyPlus. Weather data, <https://energyplus.net/weather/>; [accessed 24 November 2019].

Figure Legend

Fig. 1. Overview of the work.

Fig. 2. DSG solar power system with two-stage accumulators and RC-ORC.

Fig. 3. $T-Q$ diagram in HX1 for water-pentane.

Fig. 4. Variation of η_{PTC} with its outlet dryness.

Fig. 5. Flow chart of the HX area calculation.

Fig. 6. I_{DN} and η_{col} in a typical meteorological day in Phoenix.

Fig. 7. Reduced aperture area and the net profits for pentane.

Fig. 8. $T-Q$ diagrams in HX1: (a) water-benzene; (b) water- cyclohexane; (c) water-R1233zd-E; (d) water-MM; (e) water-R365mfc.

Fig. 9. Reduced aperture area and the net profits for benzene.

Fig. 10. Reduced aperture area and the net profits for cyclohexane and R1233zd-E.

Fig. 11. Reduced aperture area and the net profits for MM and R365mfc.

Table legend

Table 1. Summary of ORC with regenerator

Table 2. Specific parameters of PTCs and LFCs in SAM.

Table 3. Incidence angle coefficients in SAM.

Table 4. Values of constants for HX.

Table 5. Specific parameters for the DSG system.

Table 6. Parameters of the bottom cycle under nominal condition with regenerator.

Table 7. Thermodynamic performance under rated conditions without/with regenerator.

Table 8. Thermodynamic performance of the discharge process without/with regenerator.

Table 9. Parameter distribution of hot side water in heat discharge process for pentane.

Table 10. Parameters of the HXs in design condition without/with regenerator.

Table 11. Nominal conditions without/with regenerator for the five ORC fluids.

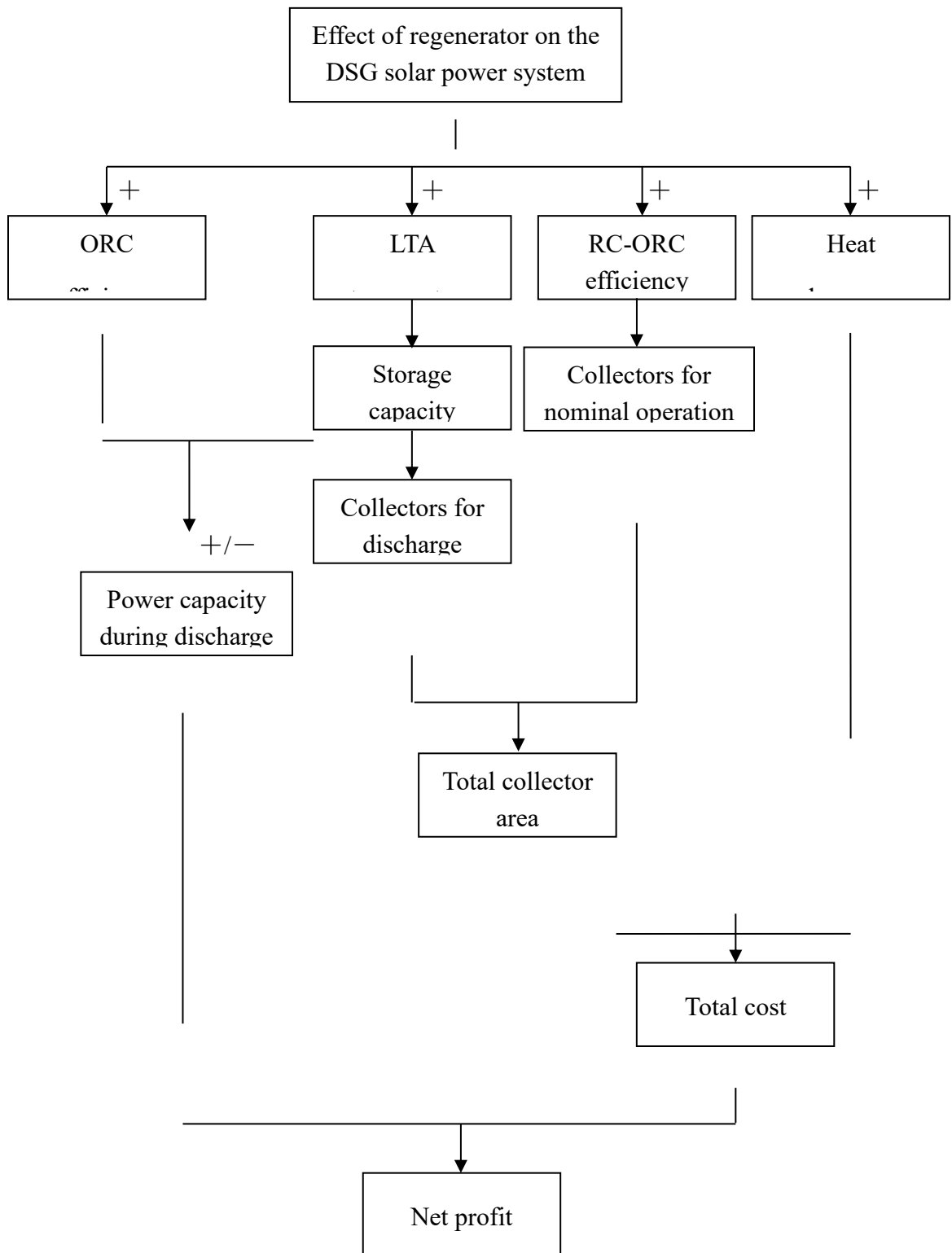
Table 12. Discharge process for the five ORC fluids.

Table 13. Parameter distribution of hot side water in the discharge process for benzene.

Table 14. Parameters of the bottom cycle under design condition with regenerator.

Table 15. Parameters of the HXs without regenerator for the five ORC fluids.

Table 16. Parameters of the HXs with regenerator for the five ORC fluids.



+/-

Fig. 1. Overview of the work.

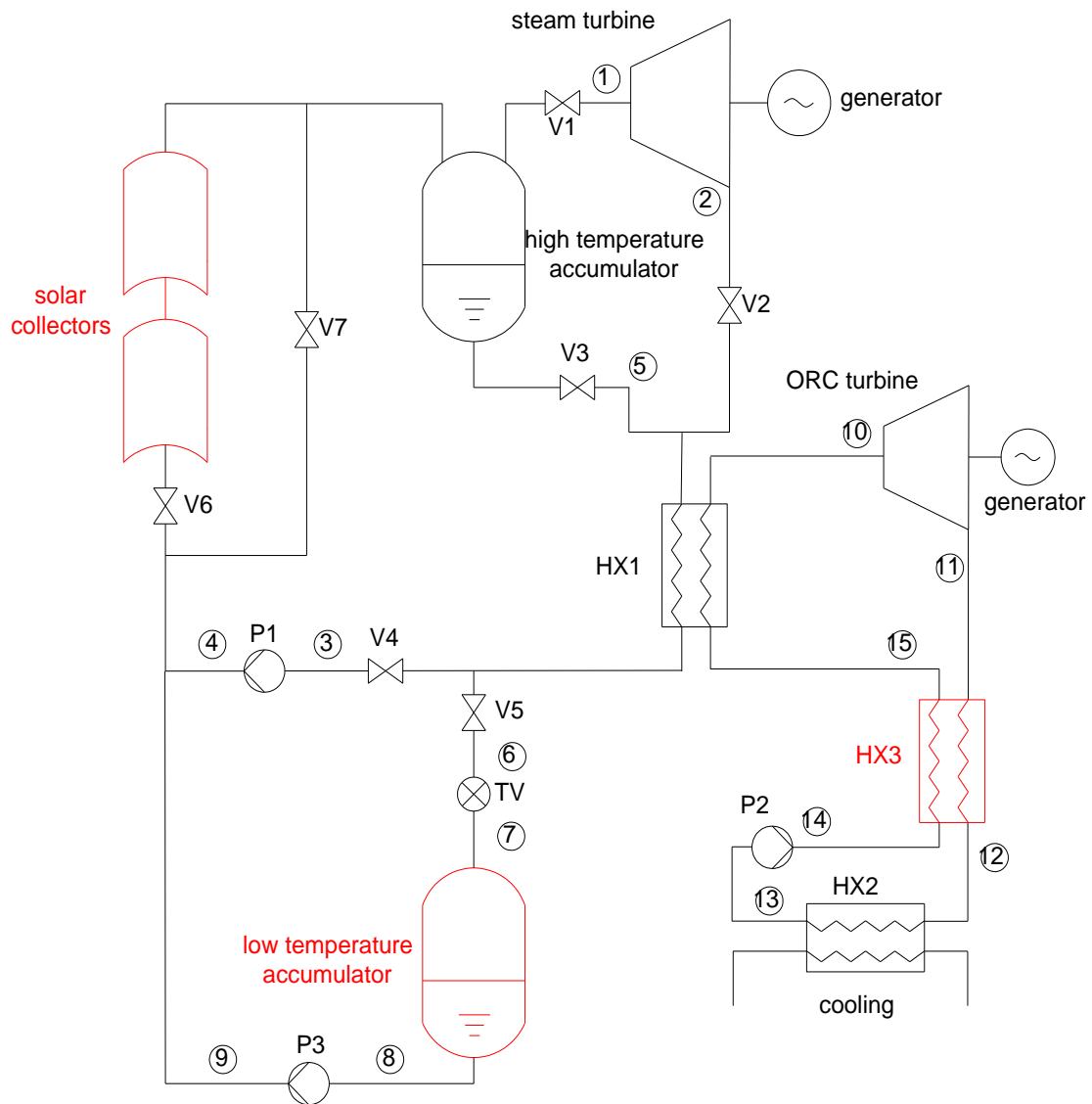


Fig. 2. DSG solar power system with two-stage accumulators and RC-ORC.

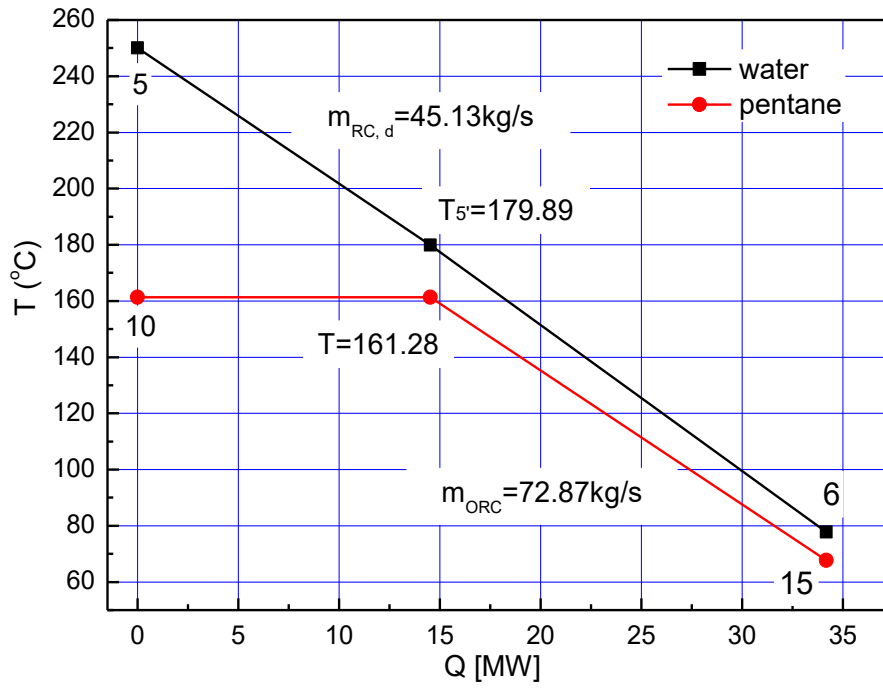


Fig. 3. T - Q diagram in HX1 for water-pentane.

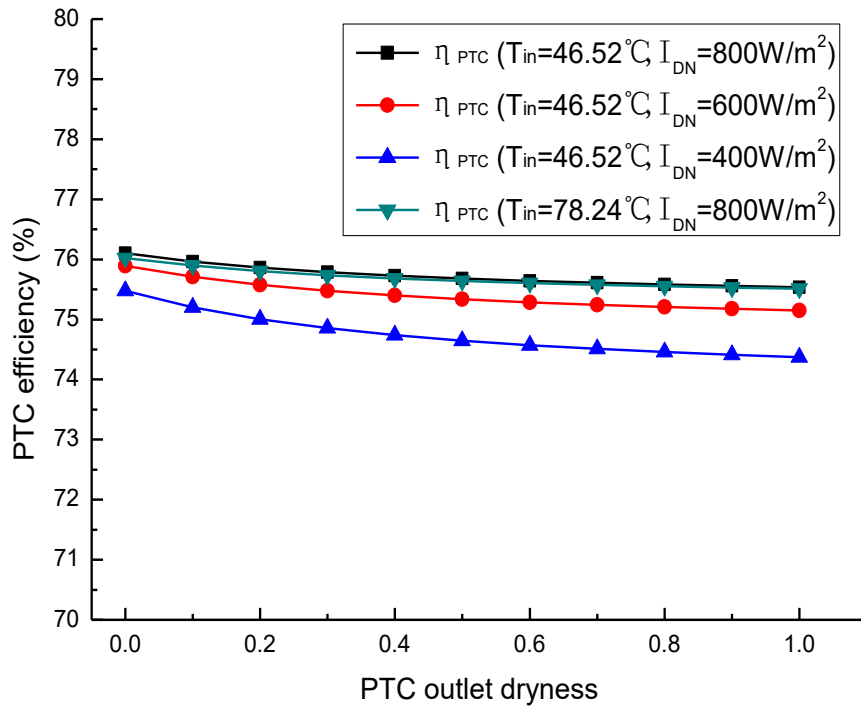


Fig. 4. Variation of η_{PTC} with its outlet dryness.

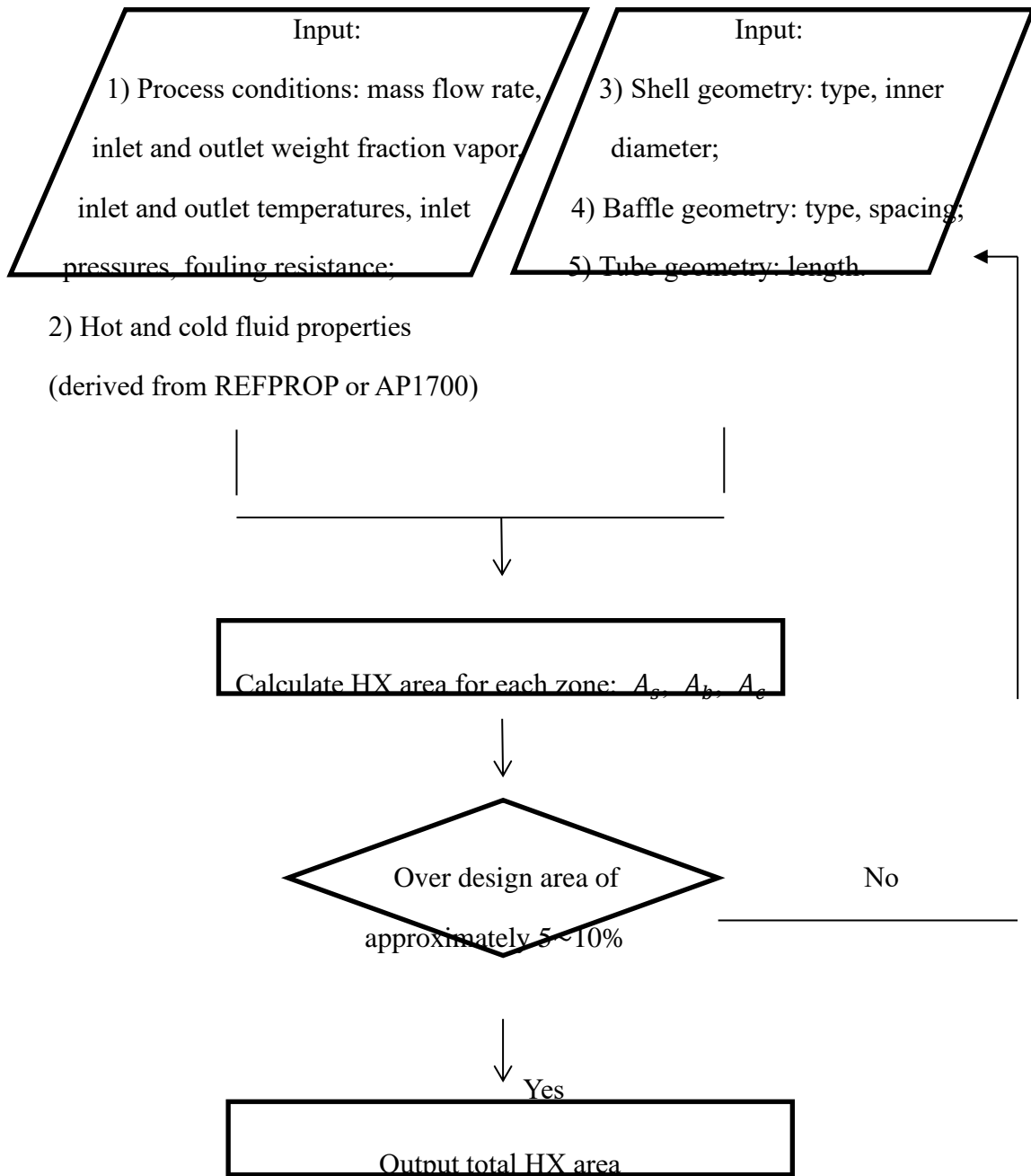


Fig. 5. Flow chart of the HX area calculation.

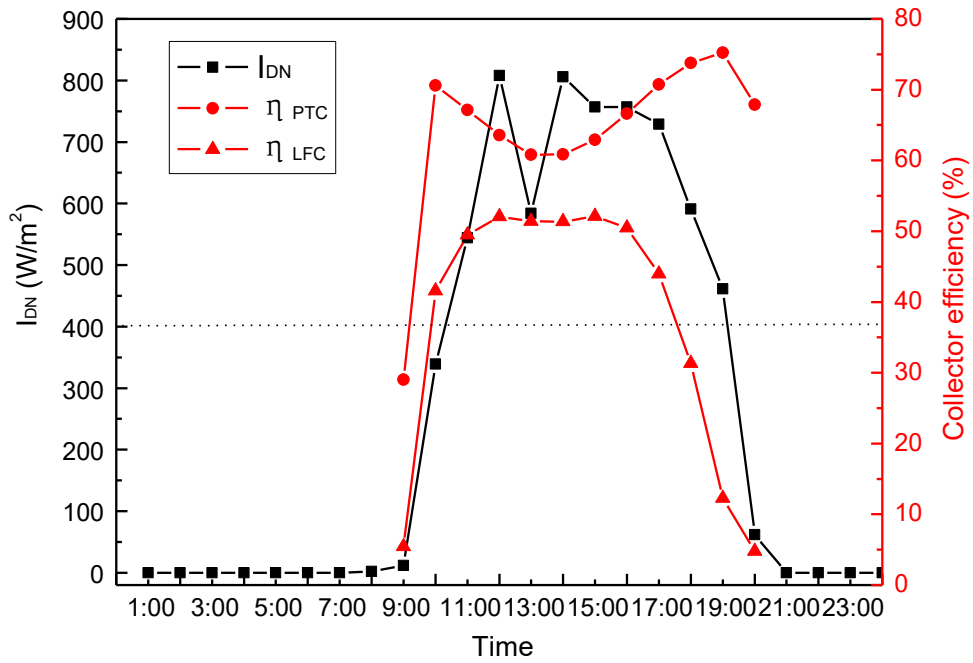


Fig. 6. I_{DN} and η_{col} in a typical meteorological day in Phoenix.

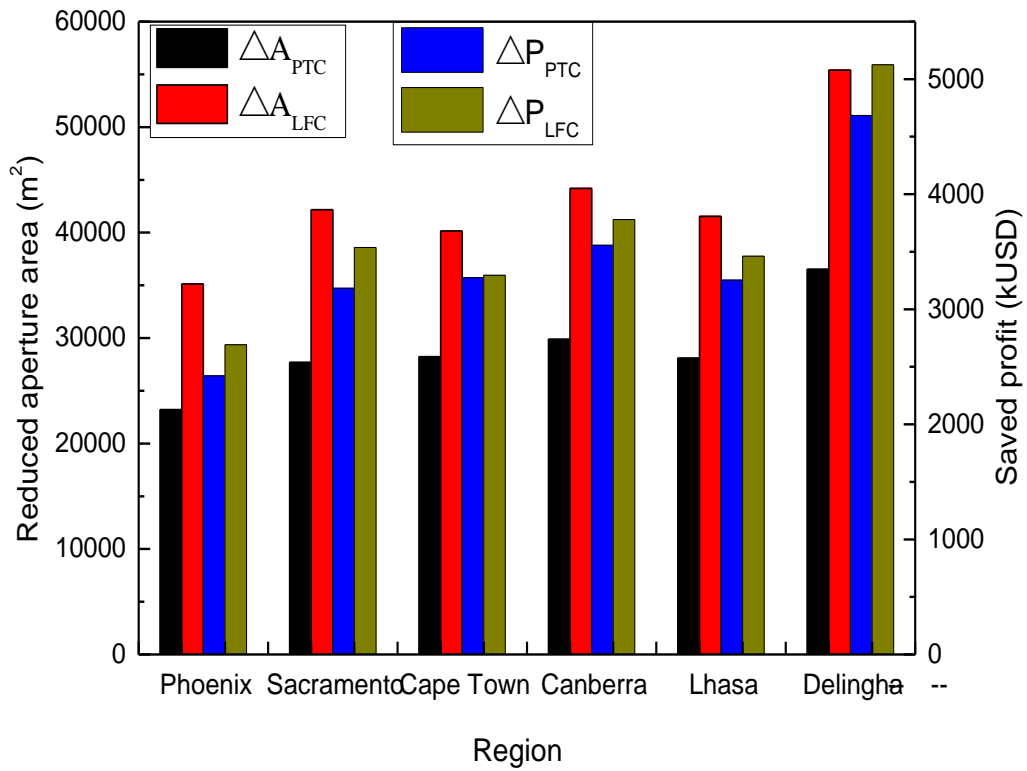
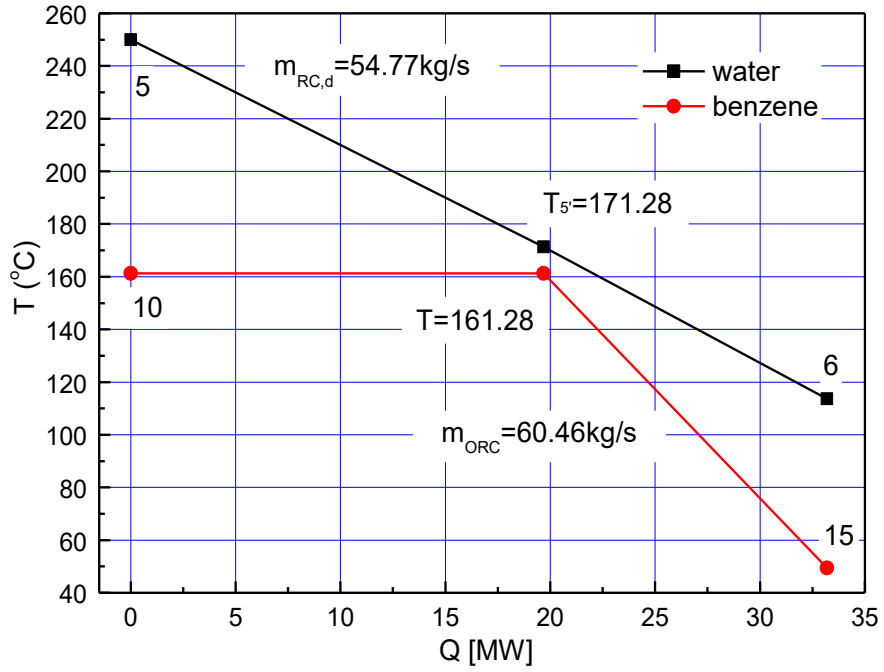
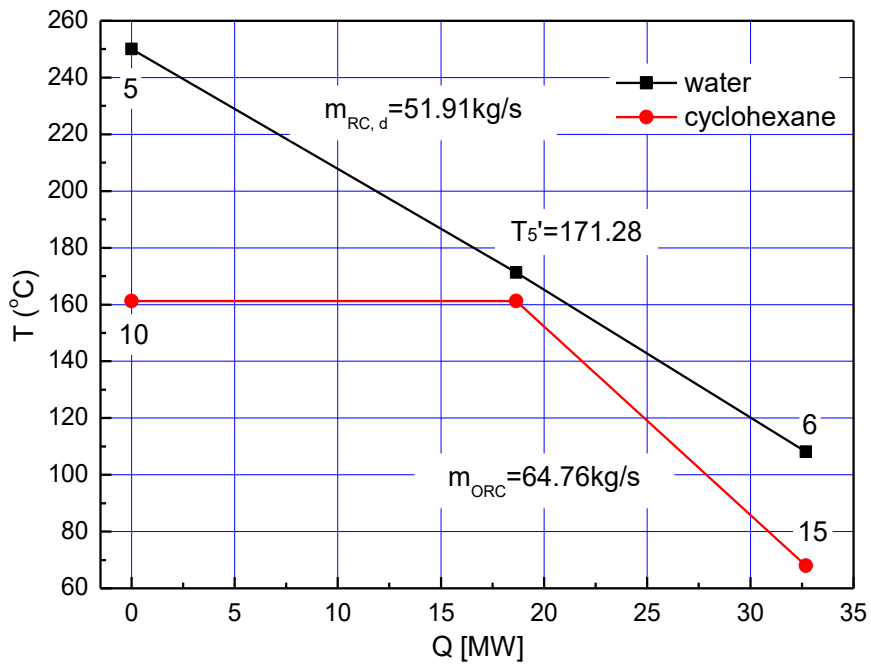


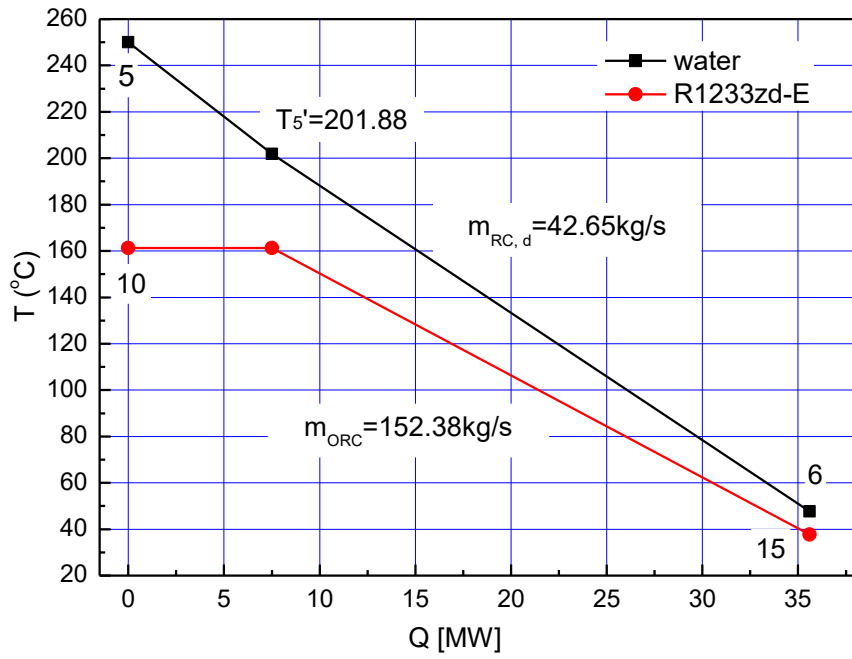
Fig. 7. Reduced aperture area and the net profits for pentane.



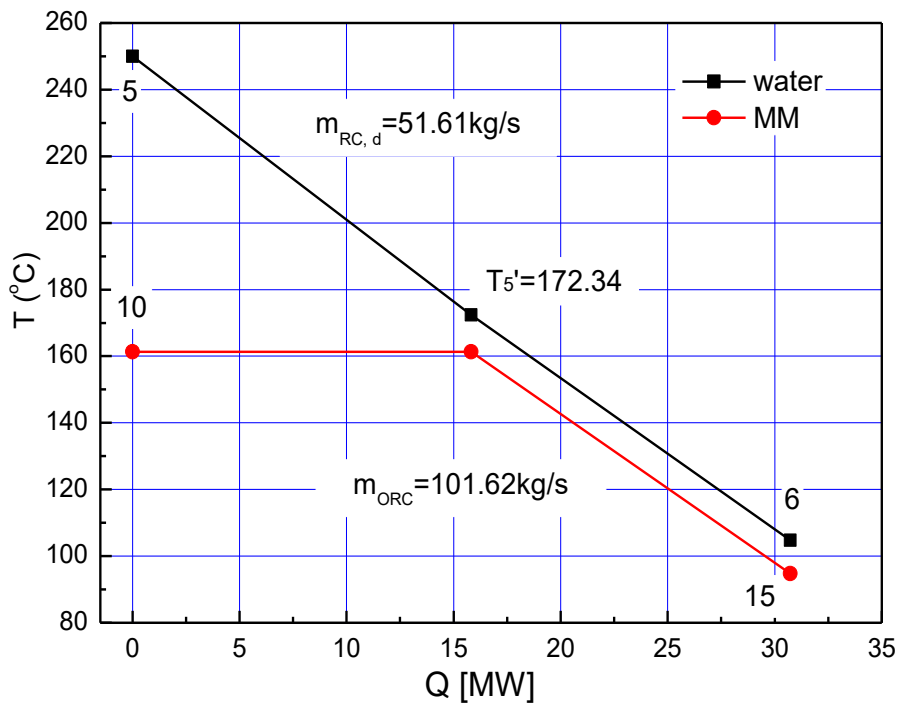
(a)



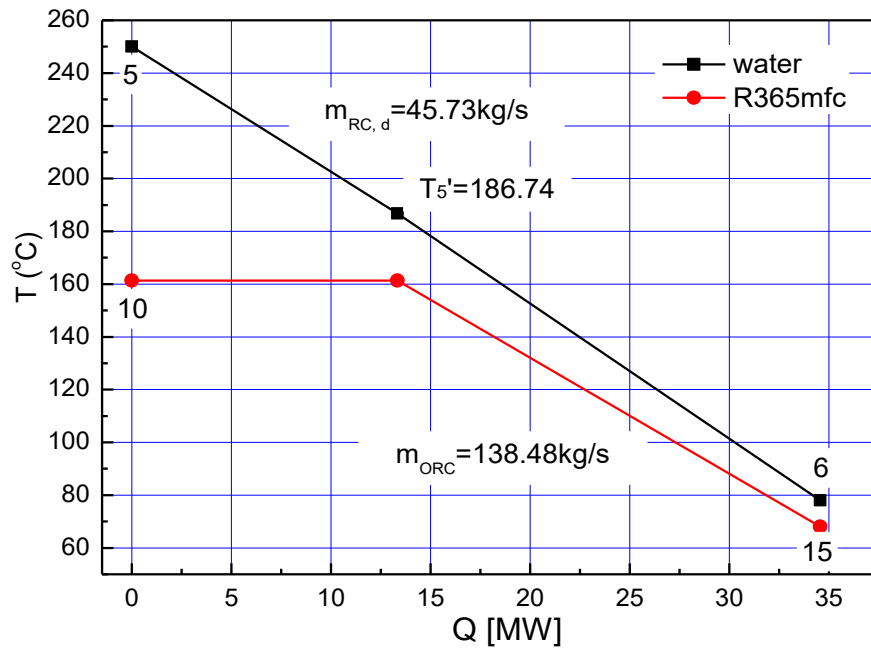
(b)



(c)



(d)



(e)

Fig. 8. T - Q diagrams in HX1: (a) water-benzene;

(b) water- cyclohexane; (c) water-R1233zd-E; (d) water-MM; (e) water-R365mfc

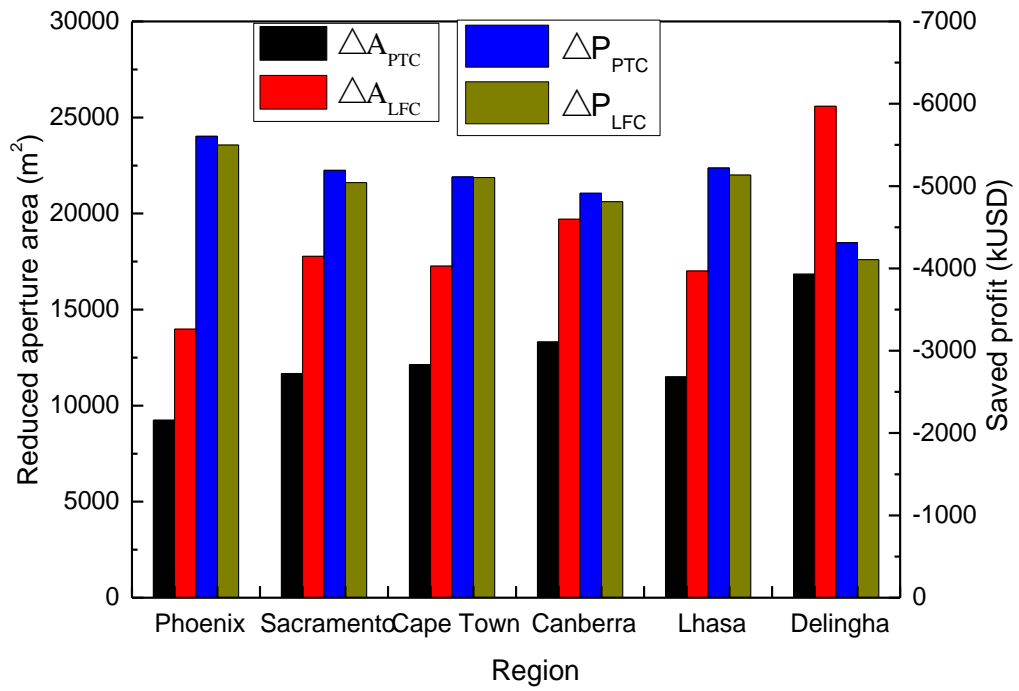


Fig. 9. Reduced aperture area and the net profits for benzene.

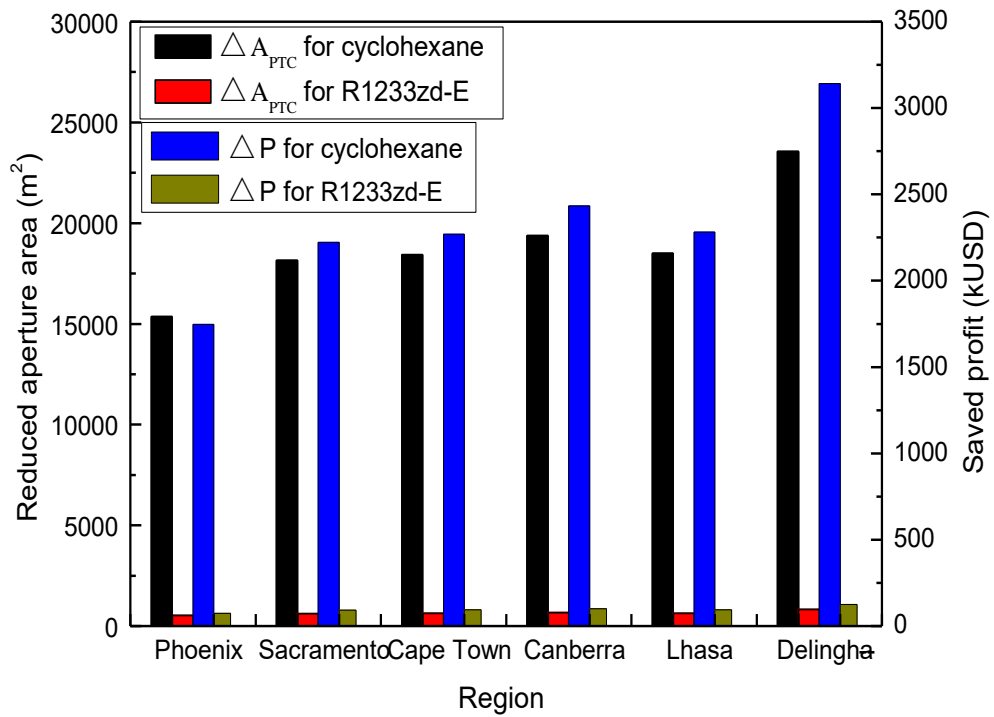


Fig. 10. Reduced aperture area and the net profits for cyclohexane and R1233zd-E.

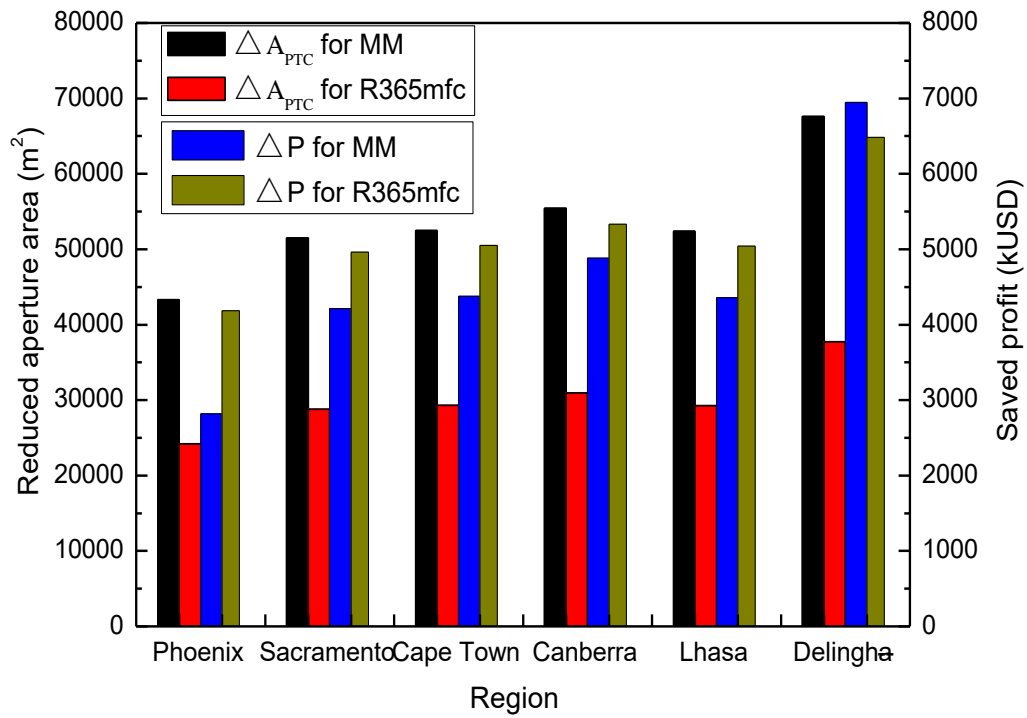


Fig. 11. Reduced aperture area and the net profits for MM and R365mfc.

Table 1. Summary of ORC with regenerator.

Results	Application	Waste heat recovery	Flue gas/ Hot stream heat recovery	Solar energy	Geothermal
	Improvements of thermodynamic indicators	Thermal efficiency	[3][4][6] [15][18]	[13][14] [17]	[19]
Exergy efficiency/ Exergy destruction		[4][6][7]	[13]	[19]	[16]
Net power output		[3][7]	[13]	[20]	[16]

Improvements of thermo-economic indicators	Payback period	[6]		
	Levelized energy cost	[6][7]	[20]	[16]
	Annual benefit		[12]	
Unfavorable in some certain conditions		[5][8]	[9][11]	
Adverse/ No impact	Net power output	[18]	[10][11]	
	Levelized energy cost		[9][13]	

Table 2. Specific parameters of PTCs and LFCs in SAM.

Terms	PTCs	LFCs
-------	------	------

Length, L	150 m	44.8 m
Aperture reflective area, A_{col}	817.5 m ²	513.6 m ²
Peak optical efficiency, $\eta_{opt,0}$	76.77%	64.31%
Heat loss coefficient, a_0		4.05
Heat loss coefficient, a_1		0.247
Heat loss coefficient, a_2		-0.00146
Heat loss coefficient, a_3		5.65e-006
Heat loss coefficient, a_4		7.62e-008
Heat loss coefficient, a_5		-1.7
Heat loss coefficient, a_6		0.0125

Table 3. Incidence angle coefficients in SAM.

c_0	1.00	$c_{0,long}$	1.003	$c_{0,trans}$	0.9896
c_1	8.84e-4	$c_{1,long}$	-0.00394	$c_{1,trans}$	7.68e-4
c_2	-5.37e-5	$c_{2,long}$	1.64e-4	$c_{2,trans}$	-2.20e-5
		$c_{3,long}$	-8.74e-6	$c_{3,trans}$	-1.24e-6
		$c_{4,long}$	6.70e-8	$c_{4,trans}$	0

Table 4. Values of constants for HX [40].

Coeffi- cient	K_1	K_2	K_3	C_1	C_2	C_3	B_1	B_2	F_M
Value	4.3247	-	0.1634	0.0388	-	0.08183	1.63	1.66	1.4
		0.303			0.11272				

Table 5. Specific parameters for the DSG system.

Term	Value	Term	Value
Steam turbine efficiency, ε_{ST}	0.75	ORC condensation temperature, T_{13}	35 °C
ORC turbine efficiency, ε_{OT}	0.82	Price of PTC [42]	170 USD/m ²
Generator efficiency, ε_g	0.95	Price of LFC [43]	120 USD/m ²
Pump isentropic efficiency, ε_p	0.75	Price of electricity [44]	0.184 USD/kWh
Minimum temperature difference, ΔT_{min}	10 °C	Reference ambient temperature, T_a	25 °C
Total volume of HTA	2500 m ³	Reference wind speed, $v_{w,ref}$	5 m/s
Total volume of LTA	2500 m ³	Reference direct normal solar irradiation, $I_{DN,ref}$	800 W/m ²

Plant life time, LT	20 years	Steam turbine inlet temperature, T_1	250 °C
Heat discharge temperature, T_5	250 °C	Steam turbine outlet pressure, P_2	0.817 MPa

Table 6. Parameters of the bottom cycle under nominal condition with regenerator.

Working fluid	State point	Pressure (kPa)	Temperature (°C)	Quality (%)
Pentane	10	1928.8	161.28	100
	11	97.70	87.11	superheated vapor
	12	97.70	46.07	superheated vapor
	13	97.70	35	0
	14	1928.8	36.07	subcooled liquid
	15	1928.8	67.71	subcooled liquid

Table 7. Thermodynamic performance under rated conditions without/with regenerator.

Parameter	η_{ORC}	η_{RC}	η_{RC-ORC}	\dot{W}_{RC}	\dot{W}_{ORC}	\dot{m}_{RC}	\dot{m}_{ORC}	Q_{nom}
Case	(%)	(%)	(%)	(MW)	(MW)	(kg/s)	(kg/s)	(MW)

)
Without regenerator	15.78	9.77	23.92	4.08	5.92	20.18	68.67	41.81	
With regenerator	18.37	9.77	26.25	3.72	6.28	18.39	72.87	38.10	

Table 8. Thermodynamic performance of the discharge process without/with regenerator.

Parameter	t_{ORC}	$\dot{m}_{RC,d}$	$\dot{m}_{ORC,d}$	\dot{w}_{p3}	\dot{w}_{loss}	$\eta_{ORC,d}$	W_d
Case	(h)	(kg/s)	(kg/s)	(kW)	(kW)	(%)	(kWh)
Without regenerator	13.1	42.17	68.67	224.88	169.0	15.18	74906.2
With regenerator	6	45.13	72.87	243.13	8	17.66	74191.6
	12.2				183.2		
	9				4		

Table 9. Parameter distribution of hot side water in heat discharge process for pentane.

Parameter	State point	Pressure (kPa)	Temperature (°C)	Quality (%)
	5	3976.2/ 3976.2	250/ 250	0/ 0
	6	3976.2/ 3976.2	46.07/ 77.71	subcooled liquid/ subcooled liquid
Without/ with	7	10.13/ 43.18	46.07/ 77.71	0.14/ 0.14

regenerator	8	10.13/ 43.18	46.07/ 77.71	0/ 0
	9	3976.2/ 3976.2	46.52/ 78.24	subcooled liquid/ subcooled liquid

Table 10. Parameters of the HXs in design condition without/with regenerator.

Process data	Without regenerator		With regenerator		
	HX1	HX2	HX1	HX2	HX3
Shell side heat transfer coefficient, kW/m ² ·K	17.17	0.99	17.16	1.15	0.46
Shell ID, mm	1600	2100	1600	2000	1700
Shell side velocity, m/s	4.87	6.78	4.17	6.42	42.21
Tube side heat transfer coefficient, kW/m ² ·K	2.28	13.81	2.19	13.72	0.91
Tube length, m	13	14	13	14	10
Tube side velocity, m/s	1.81	3.99	1.66	3.96	0.48
Tube count	2550	4230	2550	3758	2894
Overall heat transfer coefficient, kW/m ² ·K	1.041	0.689	1.016	0.768	0.257
Heat duty, MW	36.83	31.38	34.04	27.69	5.62
Effective overall temperature difference, °C	19.7	14.3	19.0	12.6	14.0

Area, m ²	1950	3490	1950	3102	1694
Over design, %	8.58	9.72	10.66	8.73	8.68
Cost, million USD	0.732	1.236	0.732	1.119	0.680

Table 11. Nominal conditions without/with regenerator for the five ORC fluids.

Fluid	η_{ORC} (%)	η_{RC-ORC} (%)	\dot{w}_{RC} (MW)	\dot{w}_{ORC} (MW)	\dot{m}_{RC} (kg/s)	\dot{m}_{ORC} (kg/s)	Q_{nom} (MW)
Benzene (without)	18.39	27.08	3.61	6.39	17.83	60.54	36.93
Benzene (with)	19.24	27.02	3.61	6.39	17.87	60.46	37.01
Cyclohexane (without)	17.46	25.42	3.84	6.16	18.99	61.94	39.34
Cyclohexane (with)	19.70	27.43	3.56	6.44	17.60	64.76	36.46
R1233zd-E (without)	15.13	24.54	4.60	5.40	19.67	152.12	40.75
R1233zd-E (with)	15.19	24.59	4.59	5.41	19.63	152.38	40.66
MM (without)	14.07	23.62	4.78	5.22	20.44	87.82	42.34
MM (with)	19.64	28.50	3.96	6.04	16.94	101.62	35.09
R365mfc (without)	15.25	23.45	4.16	5.84	20.59	129.52	42.65
R365mfc (with)	18.05	25.95	3.76	6.24	18.60	138.48	38.53

Table 12. Discharge process for the five ORC fluids.

Working fluid	t_{ORC} (h)	$\dot{m}_{RC,d}$ (kg/s)	\dot{w}_{p3} (kW)	\dot{w}_{loss} (kW)	$\eta_{ORC,d}$ (%)	W_d (kWh)	ϵ_r (%)
------------------	------------------	----------------------------	------------------------	--------------------------	-----------------------	----------------	---------------------

Benzene (without)	10.89	50.96	287.92	205.57	17.57	66474.2	—
Benzene (with)	10.13	54.77	291.94	221.40	18.36	61736.4	44.97
Cyclohexane (without)	11.17	49.65	281.35	194.53	16.66	65677.8	—
Cyclohexane (with)	10.69	51.91	280.31	208.68	18.84	65833.9	60.95
R1233zd-E (without)	12.56	42.58	227.11	170.33	14.49	64949.3	—
R1233zd-E (with)	12.55	42.65	228.02	171.02	14.55	64953.9	6.48
MM (without)	12.15	44.07	224.93	176.50	13.47	60653.0	—
MM (with)	10.37	51.61	278.69	208.50	18.73	59683.3	71.75
R365mfc (without)	12.90	43.00	244.81	172.00	14.61	72117.0	—
R365mfc (with)	12.13	45.73	247.55	184.75	17.33	72671.6	61.18

Table 13. Parameter distribution of hot side water in the discharge process for benzene.

Parameter Case	State point	Pressure (kPa)	Temperature (°C)	Quality (%)
	5	3976.2/3976.2	250/250	0/0
Without/with regenerator	6	3976.2/3976.2	95.62/113.67	subcooled liquid/ subcooled liquid
	7	86.56/161.97	95.62/113.67	0.13/0.12
	8	86.56/161.97	95.62/113.67	0/0
	9	3976.2/3976.2	96.26/114.28	subcooled liquid/ subcooled liquid

Table 14. Parameters of the bottom cycle under design condition with regenerator.

Working fluid	State point	Pressure (kPa)	Temperature (°C)	Quality (%)
Benzene	10	728.08	161.28	100
	11	19.79	66.65	superheated vapor
	12	19.79	45.33	superheated vapor
	13	19.79	35	0
	14	728.08	35.33	subcooled liquid
	15	728.08	49.42	subcooled liquid

Table 15. Parameters of the HXs without regenerator for the five ORC fluids.

Process data	Working fluid	Overall heat	Velocity,	Heat	Effective	Area	Over	Cost,
		transfer coefficient, kW/m ² ·K	m/s (shell/ tube side)	duty, MW	temperature difference, °C	, m ²	design , %	million USD
Benzen	HX1	0.461	2.33/ 1.85	33.35	15.1	5198	8.74	1.671
-e	HX2	0.729	14.49/4.24	27.87	12.9	3151	6.15	1.134
Cycloh	HX1	0.758	3.63/ 3.30	34.65	16.3	2989	6.57	1.031
-exane	HX2	0.120	41.22/2.86	16.76	34.6	4465	10.76	1.533
R1233 zd-E	HX1	1.163	5.14/ 1.13	35.45	24.5	1340	7.81	0.554
	HX2	0.679	2.24/ 4.14	30.83	13.0	3685	5.79	1.295
MM	HX1	0.768	4.78/ 3.59	36.77	19.8	2613	8.34	0.923
	HX2	0.513	31.43/4.34	31.31	16.7	3919	7.52	1.366
R365m	HX1	1.030	5.42/ 1.68	37.57	20.9	1845	5.96	0.701

-fc	HX2	0.570	3.95/ 3.58	32.01	14.4	4267	9.30	1.472
-----	-----	-------	------------	-------	------	------	------	-------

Table 16. Parameters of the HXs with regenerator for the five ORC fluids.

Working fluid	Process data	Overall heat transfer coefficient,	Velocity,	Heat duty,	Effective temperature difference,	Area,	Over design , %	Cost, million USD
		kW/m ² ·K	(shell/ tube side) m/s	MW	°C	m ²		
Benzen-e	HX1	0.464	2.27/1.94	32.66	14.3	5198	5.96	1.671
	HX2	0.818	15.33/4.41	26.31	12.7	2671	5.12	0.989
	HX3	0.070	34.29/0.26	1.44	8.0	2736	6.95	0.957
	HX1	0.782	3.21/3.79	32.11	14.7	2989	6.68	1.031

Cyclohexane	HX2	0.814	28.72/3.92	25.85	12.4	2725	6.36	1.005
	HX3	0.060	41.90/0.16	4.19	14.8	4971	5.53	1.601
R1233zd-E	HX1	1.163	5.10/1.11	35.38	24.5	1340	8.03	0.554
	HX2	0.756	4.33/4.88	29.80	12.5	3327	5.95	1.187
	HX3	0.421	37.14/1.07	0.13	10.1	63.3	103.4	0.129
MM	HX1	0.827	3.65/ 5.49	30.57	15.1	2613	6.64	0.923
	HX2	0.663	24.68/3.69	24.38	12.6	3151	7.67	1.134
R365-mfc	HX3	0.077	0.06/45.9	12.14	15.4	11098	8.58	3.473
	HX1	1.085	4.68/1.97	33.94	18.2	1845	7.33	0.701
	HX2	0.677	3.29/ 3.54	35.13	12.5	3513	6.76	1.243
	HX3	0.193	31.06/0.28	6.33	14.4	2424	6.63	0.903

Nomenclature		Abbreviation	
<i>A</i>	aperture /heat exchanger area, m ²	CEPCI	Chemical Engineering Plant Cost Index

<i>a</i>	heat loss coefficient		
<i>AST</i>	apparent solar time, min	DSG	direct steam generation
<i>B</i>	coefficient	HTA	high temperature accumulator
<i>Bo</i>	boiling number	HX	heat exchanger
<i>C</i>	cost, \$ /coefficient	IAM	incidence angle modifier
<i>c</i>	incidence angle coefficient	LFC	linear Fresnel collector
<i>ET</i>	equation of time, min	LT	lifetime
<i>d</i>	hydraulic diameter, m	LTA	low temperature accumulator
<i>F</i>	correction factor	ORC	organic Rankine cycle
<i>f</i>	Darcy resistance coefficient	P	pump
<i>G</i>	mass flux, kg/(m ² • s)	PTC	parabolic trough collector
<i>h</i>	enthalpy, kJ/kg	RC	steam Rankine cycle
<i>I</i>	solar irradiance, W/m ²	RC-ORC	steam-organic Rankine cycle
<i>K</i>	incidence angle modifier factor	RC	steam Rankine cycle
<i>k</i>	thermal conductivity, W/(m • K)	SAM	System Advisor Model
<i>LL</i>	longitude of local area, °	TV	throttle valve
<i>LST</i>	local standard time, min	V	valve

M	mass, kg	ΔT	temperature difference
\dot{m}	mass flow rate, kg/s	<i>Subscript</i>	
n	n^{th} day of a year	$0 \dots 15$	number
P	price/profit, \$	a	ambient
p	pressure, MPa	av	average
Pr	Prandtl number	b	boiling, binary
Q	heat, kJ	BM	bare module
q	receiver heat loss, W/m	c	condensation
Re	Reynolds number	col	collector
SL	standard meridian for local time zone, °	d	heat discharge
		DN	direct normal
T	temperature, °C	e	electricity
t	time duration, h	g	generator
U	heat transfer coefficient	in	inlet
v	speed, m/s	l	liquid
W	work, kWh	m	mean
\dot{w}	work, kW	M	material

Y	yield, \$	<i>min</i>	minimum
α	altitude angle, °	<i>net</i>	net power
γ	azimuth angle, °	<i>nom</i>	nominal
δ	solar declination, °	<i>OT</i>	ORC turbine
ε	device efficiency, %	<i>opt</i>	optical
η	efficiency, %	<i>out</i>	outlet
θ	incidence angle, °	<i>p</i>	pressure
ϕ	geographic latitude, °	<i>r</i>	regenerator
μ	dynamic viscosity, Pa • s	<i>ref</i>	reference
ρ	density, kg/m ³	<i>s</i>	solar, single-phase
ω	solar hour angle, °	<i>ST</i>	steam turbine
χ	quality	<i>trans</i>	transverse angle
		<i>v</i>	vapor
		<i>w</i>	water/wind